

One-Phase and Two-Phase Flow in Highly Permeable Porous Media

Yohan Davit^a, Michel Quintard^{a,*}

^a*Institut de Mécanique des Fluides de Toulouse (IMFT) - Université de Toulouse, CNRS-INPT-UPS, Toulouse
FRANCE*

*Corresponding author: Michel Quintard, Institut de Mécanique des Fluides de Toulouse (IMFT) - Université de Toulouse, CNRS-INPT-UPS, Toulouse FRANCE
Email address: michel.quintard@imft.fr, Tel. +33 5 34 32 29 21

Abstract

Many industrial and natural processes involve flow in highly permeable media, such as heat and mass exchangers, canopies or networks of urban canyons. As the flow regime in porous media is strongly dependent upon the distribution of pore sizes, the traditional assumptions used for modeling and upscaling flow equations in low permeability structures may not hold for these systems with very large pores. Reynolds numbers may be large enough so that Darcy's law is no longer valid. Capillary and Bond numbers may also be sufficiently large to invalidate the quasistatic assumptions implicit in many empirical formulations and used in upscaling multiphase flows. Here, we review several approaches that have been developed to handle such cases, basing our analysis on new experimental data and results from upscaling methods. We start by discussing the case of one-phase flow, which has been largely studied from various point of views. This has led to a variety of formulations of macro-scale momentum transport including the generalized Forchheimer equation and macro-scale turbulent models. We then go on to present the case of two-phase flows, which is a lot more complicated and mostly remains an open problem. We discuss possible ways towards deriving macro-scale models from the pore-scale equations and introduce several macro-scale models: generalized Darcy's laws, models with cross terms accounting for the viscous interaction between the two flowing phases, formulations capturing inertial or dynamic effects. Classes of models suitable for describing flow in structured media like, for instance, chemical exchangers containing structured packings are also introduced. Finally, we present hybrid representations that couple approaches at two different scales, for instance a meso-scale network approach coupled with dynamic rules obtained from pore-scale numerical simulations or experiments. This approach proved useful in describing the apparent diffusion of impinging jets in packed beds, which is often not described properly by capillary diffusion effects.

Introduction

Current trends in porous media physics involve research on transport in structures with pores at both extremes of the size spectrum. One extreme corresponds to small pore sizes and very low permeabilities, such as oil-shales or nanoporous materials. The other extreme, which is the topic of this review, corresponds to highly permeable media with a pore size that can be much larger than the capillary lengths of the fluids. This is the case for many porous media used in chemical engineering, such as trickle beds—particles larger than the millimeter—or structured packings—pore size of about 1cm. Other examples include fractured materials or geophysical formations, very coarse sands, natural and manmade canopies, nuclear reactors as well as debris beds in damaged nuclear cores. Although highly permeable porous media are of interest in many different fields, they have been given much less emphasis than low and medium permeability media.

In classical applications, macro-scale models are developed using a series of assumptions about the order of magnitudes of the relevant dimensionless numbers. For instance, one-phase flow are mostly considered in the limit where the Reynolds number (Re) goes to zero, this leading to the classical Darcy's law [1]. In the case of two-phase flow in porous media, Reynolds (Re), Bond (Bo) and capillary (Ca) numbers are often assumed to be small. This assumption is central to the validity of the so-called generalized Darcy's laws as introduced by [2].

Can we modify the macro-scale models to describe situations where one or all of these dimensionless numbers become very large? This problem has been the subject of intensive research in the past decades. Here, we review this work and discuss multiple aspects of the multiscale problems associated with one- and two-phase flow in highly permeable porous media. We put the emphasis on the structure of macro-scale models that have been developed and do not present other important issues, such as numerical modeling or experimental techniques that are specific to the highly permeable case.

Definitions, hypotheses and upscaling techniques

[Figure 1 about here.]

A variety of approaches¹ have been proposed in the literature to obtain macro-scale representations directly from the pore-scale problem. A representative sample of papers includes, among hundreds of relevant papers, the following works: [7, 8], [9, 10], [11] for volume averaging, [12], [13]), [14] for homogenization theory, [15], [16], [17] for stochastic approaches. In general, these methods apply to discretely hierarchical porous media and assume the existence of a Representative Elementary Volume of characteristic length r_0 . Many conditions must be fulfilled in order to obtain well-behaved average quantities, in particular smooth and differentiable fields in which high frequency fluctuations have been filtered out. One fundamental condition is the separation of length scales, which is often written as

$$l_p, l_\sigma \ll r_0 \ll L \quad (1)$$

where l_p and l_σ are pore-scale characteristic lengths and L is the length of the macroscopic domain (see Fig. 1). Here, the subscript p in l_p refers to the pore-space, which can be filled with either one or two fluid phases. The inequalities Eq. 1 are essentially geometrical constraints, which is only an order of magnitude estimate. In a more precise presentation, the length-scales characterize the variation of physical variables, such as pressure and velocity fields, not of geometrical features of the porous structure. For instance, L is often associated to the characteristic length of spatially averaged quantities and the validity of the hypothesis of separation of scales is process and operator dependent. In the remainder of this paper, we assume that this assumption is valid for the different configurations and flow regimes. In addition to the separation of scales, there are also other conditions that are more specific to the type of averaging that is performed. For spatial averaging for example, well-behaved averaged fields are obtained through spatial convolutions and multiple averaging techniques, see more details in [18, 19, 20, 21, 22, 23]. This is beyond the scope of this review to provide the background about all these upscaling methods.

Here, the emphasis is on results specific to the case of highly permeable media, with references

¹One may look at [3], [4], [5], [6] for a comparison between the various techniques.

to the relevant literature on upscaling. In order to clarify the physical nature of the macro-scale fields introduced in the various models, we use the vocabulary and definitions of the volume averaging technique. We define the total and superficial spatial averages using the most simple mathematical apparatus²,

$$\langle \psi_\beta \rangle = \frac{1}{V} \int_{V_\beta} \psi_\beta dV \quad (2)$$

where V_β is the volume of the β -phase contained within V , the averaging volume represented in Fig. 1, and ψ_β is a physical variable associated to the β -phase (e.g. pressure or concentration). The average of the β -phase indicator (a field having the value 1 in the β -phase, 0 elsewhere), denoted γ_β , yields

$$\varepsilon_\beta = \langle \gamma_\beta \rangle = \frac{1}{V} \int_{V_\beta} dV = \frac{V_\beta}{V} \quad (3)$$

where ε_β is the β -phase volume fraction (porosity if this is the only phase in the pore-space). This can be used to define the intrinsic phase average, $\langle \psi_\beta \rangle^\beta$ as

$$\langle \psi_\beta \rangle = \varepsilon_\beta \langle \psi_\beta \rangle^\beta \quad (4)$$

Finally, the porosity, ε , is defined as

$$\varepsilon = 1 - \varepsilon_\sigma \quad (5)$$

and the saturation of the β -phase, S_β , by

$$\varepsilon_\beta = \varepsilon S_\beta \quad (6)$$

with $S_\beta \in [0, 1]$.

²See the cited literature for a more thorough discussion and more general definitions using convolutions.

One-Phase Flow

Let us consider the flow of a fluid (β -phase) within a porous structure (solid phase σ) with the fluid filling the entire pore space. The pore-scale problem describing the flow may be written for a Newtonian fluid with constant density, ρ_β , and viscosity, μ_β , as

$$\nabla \cdot \mathbf{v}_\beta = 0 \text{ in } V_\beta \quad (7)$$

$$\rho_\beta \frac{\partial \mathbf{v}_\beta}{\partial t} + \rho_\beta \mathbf{v}_\beta \cdot \nabla \mathbf{v}_\beta = -\nabla p_\beta + \rho_\beta \mathbf{g} + \mu_\beta \nabla^2 \mathbf{v}_\beta \text{ in } V_\beta \quad (8)$$

$$\text{B.C.1} \quad \mathbf{v}_\beta = 0 \quad \text{at } A_{\beta\sigma} \quad (9)$$

where \mathbf{v}_β and p_β are the fluid velocity and pressure respectively, g is the gravitational acceleration, and $A_{\beta\sigma}$ represents the interface between the fluid and solid phases.

The macro-scale variables needed for describing the flow of the β -phase are the intrinsic phase averaged pressure

$$P_\beta = \langle p_\beta \rangle^\beta \quad (10)$$

and the filtration velocity, \mathbf{V}_β , or intrinsic velocity, \mathbf{U}_β , defined as

$$\mathbf{V}_\beta = \langle \mathbf{v}_\beta \rangle = \varepsilon_\beta \langle \mathbf{v}_\beta \rangle^\beta = \varepsilon_\beta \mathbf{U}_\beta \quad (11)$$

For one-phase flow of a Newtonian fluid, the important dimensionless parameter characterizing the flow is the pore-scale Reynolds number, which can be defined as

$$\text{Re} = \frac{\rho_\beta U_r l_\beta}{\mu_\beta} \quad (12)$$

where U_r is a reference velocity, often the intrinsic average velocity, and l_β a pore-scale characteristic length. We can use the Reynolds number to distinguish different flow regimes [24] corresponding to different macro-scale models.

Creeping Flow

In the limit $Re \rightarrow 0$ (creeping flow) there is a broad consensus for Darcy's law [1], provided that the separation of scales holds. This reads

$$\mathbf{V}_\beta = -\frac{1}{\mu_\beta} \mathbf{K} \cdot (\nabla P_\beta - \rho_\beta \mathbf{g}) \quad (13)$$

where \mathbf{K} is the intrinsic permeability tensor. This equation, together with the macro-scale version of the mass balance equation,

$$\nabla \cdot \mathbf{V}_\beta = 0, \quad (14)$$

can be used to calculate the macro-scale velocity and pressure fields.

This macro-scale law is supported by many experimental results, in particular by Darcy's own experiments. It is also confirmed by theoretical developments. Upscaling Stokes equations at the pore-scale (Eqs. 7–9) via homogenization theory [25] or volume averaging [26, 20] yields a sound physical basis for the use of Darcy's law. Key steps of the mathematical developments are as follows.

- Linearization of the Navier-Stokes equations in the limit $Re \rightarrow 0$ to obtain Stokes' problem,
- Introduction of a coupled problem for macro-scale values and pore-scale deviations defined as

$$p_\beta = P_\beta + \tilde{p}_\beta \quad ; \quad \mathbf{v}_\beta = \mathbf{U}_\beta + \tilde{\mathbf{v}}_\beta \quad (15)$$

- Simplifications of the problem based on the separation of spatial scales,
- Introduction of an approximated solution of the coupled problem through a *closure*, which emerges from the mathematical structure of the Stokes problem. At first-order, this closure reads

$$\tilde{p}_\beta = \mu_\beta \mathbf{b} \cdot \mathbf{U}_\beta \quad ; \quad \tilde{\mathbf{v}} = \mathbf{B} \cdot \mathbf{U}_\beta \quad (16)$$

where the vector \mathbf{b} and tensor \mathbf{B} are called mapping variables. These are solutions of a local

problem that is usually solved over a representative unit cell (see a),

- Derivation of the macro-scale equation from the averaged equations and the closure: one obtains Darcy's law, Eq. 13 and the intrinsic permeability, given by:

$$\mathbf{K}^{-1} = -\varepsilon_{\beta}^{-2} \frac{1}{V} \int_{A_{\beta\sigma}} \mathbf{n}_{\beta\sigma} \cdot (-\mathbf{Ib} + \nabla \mathbf{B}) dA \quad (17)$$

which is calculated from the solution of the closure problem over the representative unit cell. Nowadays, this is almost a routine operation to calculate such effective properties from reconstructed 3D images, such as those obtained using x-ray microtomography.

Inertial Effects for Moderate Reynolds Numbers

[Figure 2 about here.]

When the Reynolds number becomes sufficiently large, inertial effects start to predominate and the relation between the pressure drop and the average velocity becomes nonlinear. While the exact definition of the different regimes is still a matter of controversy [27, 28, 29, 30, 31], the apparent permeability that would reproduce the actual pressure-velocity relation may be roughly described as in Fig. 2. The first nonlinear regime corresponds to a cubic dependence of the pressure drop upon the Reynolds number $\propto \text{Re}^3$. This regime is often called the *weak inertial regime*, as inertial effects affect the drag but the flow is still laminar and steady. As the Reynolds number is increased beyond this regime, a *strong inertial regime* is usually observed that also corresponds to a steady flow but for which the pressure drop can be approximated as $\propto \text{Re}^n$ with $1 \leq n \leq 2$. The exact value of n is difficult to evaluate. In the literature so far, n seems to depend upon the structure and order of the porous medium. For instance, the work in [31] indicates that the value of n is closer to 2 for disordered media than for order ones. Further, for some porous structures—maybe most of them—a single value of n cannot be defined [32] and the strong inertial regime seems to correspond to a transition regime. For even larger Reynolds numbers, a transition to unsteady flow occurs. When this happens, time fluctuations of the pressure and velocities must be considered. In this Section,

we limit our analysis to the onset of unsteady flows and small temporal fluctuations. We therefore neglect time fluctuations and concentrate on spatial averaging (we will see in Section a how to deal with large temporal fluctuations.). Recent work in [32] suggests that the onset of unsteady flow corresponds to a quadratic regime and to a classical Forchheimer equation.

This has led to the proposal of heuristic laws having the form of a Forchheimer equation, which can be written in a very general manner as

$$0 = -\nabla P_\beta + \rho_\beta \mathbf{g} - \mu_\beta \mathbf{K}^{-1} \cdot \mathbf{V}_\beta - \mathbf{F}(\mathbf{V}_\beta) \cdot \mathbf{V}_\beta \quad (18)$$

where the term $\mathbf{F}(\mathbf{V}_\beta) \cdot \mathbf{V}_\beta$ is called a generalized Forchheimer term in reference to the work in [33]. If one solves the upscaling problem using an asymptotic expansion in terms of Reynolds number, we can recover theoretically the first correction to Darcy's law, i.e., cubic terms in the weakly inertial regime [28, 27, 29, 31, 34],

$$\mathbf{F}(\mathbf{V}_\beta) \sim \|\langle \mathbf{v}_\beta \rangle\|^2 \quad (19)$$

The correction to Darcy's law in the steady inertial regime is often relatively small (but it can be measured with accurate experimental data [35, 36, 37]). In many situations, only the quadratic correction has a significant impact and inertial effects are often well *approximated* macroscopically by a quadratic term, i.e.,

$$\mathbf{F}(\mathbf{V}_\beta) \sim \|\langle \mathbf{v}_\beta \rangle\|. \quad (20)$$

This is supported by experimental data [33, 35, 38, 36, 39, 37] as well as numerical predictions [31, 40]. However, from a fundamental perspective, the quadratic expression of the drag is only an approximate description of momentum transport. Calculations over simple unit cells [31] indicate that there are, in fact, many transitional regimes. This implies that, in general, a careful analysis of the regime and the accuracy required in a specific application must be performed before deciding whether to use a simple quadratic correction or more complex descriptions.

The above expression of macroscale momentum transport, which involves a tensorial expression of \mathbf{F} , also suggests the potential existence of anisotropy effects for the Forchheimer term. Simpler expressions are often used in the engineering practice, like Ergun's equation [35] which reads

$$0 = -\nabla P_\beta + \rho_\beta \mathbf{g} - \mu_\beta K^{-1} \mathbf{V}_\beta - \rho_\beta \eta^{-1} \|\mathbf{V}_\beta\| \mathbf{V}_\beta \quad (21)$$

where η is called the *passability*. Based on collected experimental data, Ergun proposed the following correlations for K and η in the case of packed beds which are used frequently in the engineering practice

$$K = \frac{\varepsilon^3 d^2}{h_K (1 - \varepsilon)^2} \quad ; \quad \eta = \frac{\varepsilon^3 d}{h_\eta (1 - \varepsilon)} \quad (22)$$

where d is the equivalent particle diameter and $h_K = 150$ and $h_\eta = 1.75$. Such formulas must be corrected for particles that are not spherical, as shown in [37].

In conclusion, Forchheimer's law is an attractive macro-scale model that is broadly used to study many problems [41, 42, 43, 44, 45], but it also has its limitations, in particular regarding the expression of the quadratic drag law, as discussed above.

Towards Turbulence in Porous Media

When the Reynolds number becomes very large, a fundamental question is whether the flow can structure on large length scales, larger than several pores, or whether the porous structure imposes a cut-off in the cascade of length scales. This is important because this implies very different macroscale models. If the vortices and turbulent structures are localized in a single unit-cell, then we may be able to use the general Forchheimer equation, only adapting the form of the drag (see [30, 46]). If this is not the case, the macroscale model will need to account for other effects. For instance, are terms in $\mathbf{V}_\beta \cdot \nabla \mathbf{V}_\beta$ or macroscale turbulence models needed? Direct numerical simulations in [47] indicate that spatial correlations of the velocity field decrease very rapidly and that the flow is almost periodic. This suggests that the porous medium indeed induces a cut-off in the length scales characterizing the structures of the flow. Therefore, performing calculations of the flow over several unit-cells with periodic boundary conditions will reproduce accurately the

flow. On the other hand, it has been observed using direct numerical simulations that turbulence generated in a fluid layer or at the interface between fluid and porous layers may penetrate a distance of several unit cells into the porous domain and that in this area a macro-scale turbulence model is needed [48]. Transition and bifurcations may also be a lot more sensitive upon the size of the domain considered, as is shown for the unsteady transition in [49], and calculations over a single unit-cell do not yield accurate results for the critical Reynolds numbers. There are still very few studies on this problem and these seminal works open the way towards understanding and modeling trully turbulent situations.

At any rate, for large Reynolds numbers, temporal and spatial fluctuations are both important and time averaging must also be introduced. While the operators for spatial and time averaging may in principle commute [50], the application in a sequential manner, as illustrated below

$$\text{I. } \mathbf{v}_\beta \rightarrow \langle \mathbf{v}_\beta \rangle \rightarrow \overline{\langle \mathbf{v}_\beta \rangle} \quad (23)$$

$$\text{II. } \mathbf{v}_\beta \rightarrow \overline{\mathbf{v}_\beta} (\text{RANS, ...}) \rightarrow \langle \overline{\mathbf{v}_\beta} \rangle \quad (24)$$

where $\langle \varphi \rangle$ stands for the spatial averaging of a variable φ while $\overline{\varphi}$ stands for the time average, may lead to different macro-scale models. The fundamental reason is that each upscaling or averaging step introduces approximations that do not in general commute. Scheme I, favored by [51] and [52] among others, involves first spatial averaging and then, assuming that the closed macro-scale equations have the form of a generalized Forchheimer equation, it is subsequently time averaged. Since it was found that the assumption of a Forchheimer equation is difficult to justify theoretically, most researchers follow scheme II. In this case, it is assumed that the Navier-Stokes equations may be time averaged and the resulting equations are then spatially averaged [53, 54, 55, 50]). The result is in general some sort of effective RANS macro-scale model. It must be emphasized that, in the two procedures, it is difficult to justify the possibility of a decoupled closure for both averages. Also, a complete validation through experiments or numerical modeling is still an open problem and the need for such models needs to be fully assessed.

Meso-scale models for one-phase flow with pore-scale rough surfaces

In many geometries, the simple multi-scale scheme illustrated in Fig. 1 cannot be used directly in direct numerical simulations or in the upscaling algorithms because of the existence of sub-scale heterogeneities. This is the case for instance if the solid-fluid interface displays roughnesses of wavelengths much smaller than the pore-scale characteristic length, l_β , as is illustrated in Fig. 3.

[Figure 3 about here.]

In that case, one approach consists in developing a meso-scale model, intermediate between the pore-scale and the Darcy-scale. The idea is illustrated in Fig. 4. The picture on the left-hand side shows the pore-scale with the flow of the fluid satisfying a no-slip condition on the rough solid-fluid interface. If the impact of the roughness is localized to the vicinity of the wall, and if several other assumptions are satisfied (see [32] for more detail), the complex flow field near the rough interface can be approximated. When that is the case, the flow problem can be replaced by a meso-scale representation involving a smooth effective surface. The boundary condition applying to this surface is an effective boundary condition constructed so that the bulk flow in the pores is correctly approximated by the effective surface modeling. This smooth modeling is illustrated in Fig. 4 (right). Various methodologies have been proposed to develop such effective boundary conditions. For the case of Navier-Stokes equations, the reader is referred to works in [56], [57], [58] and [32]. In these studies, the effective boundary condition becomes a generalized, anisotropic Navier conditions which may be written as

$$\mathbf{v}_s = \mathbf{M} \cdot \left[\mathbf{n} \cdot \left(\nabla \mathbf{v}_s + (\nabla \mathbf{v}_s)^T \right) \cdot (\mathbf{I} - \mathbf{nn}) \right], \quad (25)$$

which is satisfied on the smooth effective surface. Here, \mathbf{v}_s is the velocity on the effective surface, \mathbf{n} the normal to the interface, \mathbf{I} the unity tensor and \mathbf{M} the Navier tensor. The Navier tensor can be obtained from the resolution of an ancillary problem over a representative portion of the roughness. This tensor depends on the position of the effective surface, which can be fixed arbitrarily—although there is an optimal position minimizing the error [57, 32]. In general, the tensor does not reduce

to a scalar, for instance in the case of anisotropic corrugated surfaces [32]. This theory has been applied to simple unit cells and structured packings with rough surfaces. The results, compared with direct numerical simulations, suggest that the approach is accurate in the weak and strong inertial regime, but fails when unsteady flow develops. When this happens the effect of the roughness is not localized to a boundary layer, but propagates through the whole pore, an effect that cannot be captured by the effective surface. Of course, this is for roughnesses that are larger than the laminar sublayer, otherwise the effect remains localized.

The development of such meso-scale models is a very attractive methodology to deal with highly complex multiple-scale pore structures. This approach will also be discussed in the case of two-phase flows.

[Figure 4 about here.]

Two-Phase Flow

The pore-scale problem for two-phase flows in porous media involves mass and momentum balance equations for both phases, denoted β and γ , and boundary conditions. For simplicity and clarity, the full upscaling problem is not developed here. However, it is interesting to detail just the condition at the interface between both fluids, in order to present the physics of the problem and links with upscaling. The boundary condition for the momentum equation reads

$$\begin{aligned} & -\mathbf{n}_{\beta\gamma} p_{\beta} + \mu_{\beta} \mathbf{n}_{\beta\gamma} \cdot \left(\nabla \mathbf{v}_{\beta} + (\nabla \mathbf{v}_{\beta})^T \right) = \\ & -\mathbf{n}_{\beta\gamma} p_{\gamma} + \mu_{\gamma} \mathbf{n}_{\beta\gamma} \cdot \left(\nabla \mathbf{v}_{\gamma} + (\nabla \mathbf{v}_{\gamma})^T \right) + 2\sigma H_{\beta\gamma} \mathbf{n}_{\beta\gamma} \text{ at } A_{\beta\gamma} \end{aligned} \quad (26)$$

where σ is the interfacial tension, $H_{\beta\gamma}$ the interface curvature and $\mathbf{n}_{\beta\gamma}$ the normal. During upscaling using volume averaging, we often need to evaluate the effects of all points $\mathbf{x} + \mathbf{y}$ in the averaging volume on the average value of the field at the centroid \mathbf{x} . To do so, we can introduce Taylor series approximation (when the average field is differentiable [18, 19, 23]). For instance, the pressure

reads

$$p_\beta(\mathbf{x} + \mathbf{y}_\beta) = \left(P_\beta \Big|_{\mathbf{x}} + \mathbf{y}_\beta \cdot \nabla P_\beta \Big|_{\mathbf{x}} + O(\mathbf{y}_\beta^2) \right) + \tilde{p}_\beta(\mathbf{x} + \mathbf{y}_\beta), \quad (27)$$

where \mathbf{y}_β describes the position of a point in the β -phase relative to the centroid of some averaging volume at position \mathbf{x} . Neglecting second-order terms in $O(\mathbf{y}_\beta^2)$, the boundary condition then reads

$$\begin{aligned} & \mathbf{n}_{\beta\gamma} \left(P_\gamma \Big|_{\mathbf{x}} - P_\beta \Big|_{\mathbf{x}} \right) + \mathbf{n}_{\beta\gamma} \mathbf{y}_\beta \cdot \left[\left(\nabla P_\gamma \Big|_{\mathbf{x}} - \rho_\gamma \mathbf{g} \right) - \left(\nabla P_\beta \Big|_{\mathbf{x}} - \rho_\beta \mathbf{g} \right) + (\rho_\gamma - \rho_\beta) \mathbf{g} \right] \\ & = -\mathbf{n}_{\beta\gamma} (\tilde{p}_\gamma - \tilde{p}_\beta) + \mu_\gamma \mathbf{n}_{\beta\gamma} \cdot \left(\nabla \mathbf{v}_\gamma + (\nabla \mathbf{v}_\gamma)^T \right) - \mu_\beta \mathbf{n}_{\beta\gamma} \cdot \left(\nabla \mathbf{v}_\beta + (\nabla \mathbf{v}_\beta)^T \right) \\ & \quad + 2\sigma H_{\beta\gamma} \mathbf{n}_{\beta\gamma} \text{ on } A_{\beta\gamma} \end{aligned} \quad (28)$$

Here, we see that the curvature within the averaging volume will depend on (i) the capillary pressure ($P_\gamma \Big|_{\mathbf{x}} - P_\beta \Big|_{\mathbf{x}}$), (ii) gravity effect, (iii) viscous effects, (iv) dynamic effects (important values of the pressure deviations related to the flow or of terms like $(\nabla P_\gamma \Big|_{\mathbf{x}} - \rho_\gamma \mathbf{g}) - (\nabla P_\beta \Big|_{\mathbf{x}} - \rho_\beta \mathbf{g})$). Further, another important parameter that does not appear when considering the pointwise fluid-fluid boundary condition is the wettability of the solid phase, which can deeply influence the spatial distribution of the two phases in the pore-space, invasion patterns and the curvature of the interface [59, 60]. Depending on the assumptions used in the upscaling, several models can be developed. Their physical meaning and mathematical structure are discussed in the next sections.

Quasistatic Models for low capillary, Bond and Reynolds numbers

The first class of models that we consider assumes that the boundary condition Eq. 28 can be replaced, for small capillary and Bond numbers (surface tension dominated) defined as

$$\text{Ca} = \frac{\mu_r U_r}{\sigma} \quad ; \quad \text{Bo} = \frac{|\rho_\beta - \rho_\gamma| g r_0^2}{\sigma}, \quad (29)$$

by

$$P_\gamma \Big|_{\mathbf{x}} - P_\beta \Big|_{\mathbf{x}} = 2\sigma H_{\beta\gamma} \quad (30)$$

As a result, the interface curvature is considered locally constant. We further assumes that the temporal evolution of the interface at the pore-scale is fast compared to that of macroscale phenomena, i.e. that characteristic times of the interface movement are small compared to the relaxation of the pressure and velocity field at macroscale. Under such a *quasistatic* assumption, we can introduce a macro-scale capillary pressure condition as

$$P_\gamma - P_\beta = p_c(S_\beta, \dots) \quad (31)$$

where p_c is the capillary pressure relationship, S_β is the saturation defined by Eq. 6 and "... " is here as a reminder that the capillary pressure can depend on other macroscale parameters. Triple line and wettability effects are taken into account in the expressions for the capillary and relative permeability, which are treated as non-linear functions of the saturation. The quasistatic assumption is an hypothesis underlying most heuristic generalized Darcy's laws model classically used in engineering practice [2]. The whole model reads

$$\frac{\partial \varepsilon S_\beta}{\partial t} + \nabla \cdot \mathbf{V}_\beta = 0 \quad (32)$$

$$\mathbf{V}_\beta = -\frac{1}{\mu_\beta} \mathbf{K}_\beta \cdot (\nabla P_\beta - \rho_\beta \mathbf{g}) \quad (33)$$

$$\frac{\partial \varepsilon S_\gamma}{\partial t} + \nabla \cdot \mathbf{V}_\gamma = 0 \quad (34)$$

$$\mathbf{V}_\gamma = -\frac{1}{\mu_\gamma} \mathbf{K}_\gamma \cdot (\nabla P_\gamma - \rho_\gamma \mathbf{g}) \quad (35)$$

$$S_\beta + S_\gamma = 1 \quad (36)$$

with phase permeabilities generally written with relative permeabilities $k_{r\beta}(S_\beta)$ and $k_{r\gamma}(S_\gamma)$ as

$$\mathbf{K}_\beta = \mathbf{K} k_{r\beta}(S_\beta) \quad ; \quad \mathbf{K}_\gamma = \mathbf{K} k_{r\gamma}(S_\gamma) \quad (37)$$

The actual repartition of the phases within a porous medium is necessarily a *transient process* and the quasistatic assumption is not always valid. Transitions between steady-states, and therefore

the steady-states themselves, are affected by a variety of dynamic mechanisms such as Haines jumps [61, 62], snap-off [63, 64], viscous entrainment of droplets through constrictions [65] and a variety of other mechanisms [66, 67]. As a consequence, relative permeabilities and capillary pressures, even in the quasistatic assumption, show memory and hysteresis properties and the saturation is not the only state variable [68]. For example, using volume averaging and principles of the thermodynamics of irreversible processes, several authors proposed to use the interfacial area, $a_{\beta\gamma}$, defined as

$$a_{\beta\gamma} = \frac{1}{V} \int_{A_{\beta\gamma}} dA \quad (38)$$

as an additional independent variable [69, 70, 71, 72].

From an upscaling point of view, the major consequence of these various mechanisms is that the pore-scale repartition of the phases involves several time and length scales, with different flow patterns affecting more than a single pore. This is most obvious when studying meso-scale representations of a porous medium, in particular network models [73]—even though there is also an issue of representativity of a network model as being a realistic representation of complex porous media such as rocks. Recall that, in the absence of macro-scale inertia terms (i.e., very small Reynolds numbers)³ and gravity effects (small Bond numbers), the flow pattern depends on a capillary number and the viscosity ratio, as well as other geometrical and topological characteristics of the network model, including its large-scale length. Results show different flow patterns including viscous fingering, stable displacement, capillary fingering as illustrated by the Ca-viscosity ratio diagrams published in [59, 74] and other works including [60]. The consequence of this complexity is that it is difficult to develop a formal upscaling methodology for all cases.

For example, if we keep the viscosity terms in Eq. 28 while making the assumption of quasistaticity, small Bond and Reynolds numbers, [26, 75, 76, 77, 78, . . .] macro-scale momentum

³Many pore-scale mechanisms, such as Haines jumps, may exhibit inertial effects in the transition from one quasistatic state to another.

balance equations read

$$\mathbf{V}_\alpha = -\frac{1}{\mu_\alpha} \mathbf{K}_{\alpha\alpha} \cdot (\nabla P_\alpha - \rho_\alpha \mathbf{g}) + \mathbf{K}_{\alpha\kappa} \cdot \mathbf{V}_\kappa \quad (39)$$

$$\alpha, \kappa = \beta, \gamma \quad \alpha \neq \kappa$$

which are different from the classical Generalized Darcy's laws. In particular, the cross terms $\mathbf{K}_{\alpha\kappa}$ in these equations account for the viscous interaction between the fluid phases. These cross terms further satisfy the following relations

$$\mu_\beta \mathbf{K}_{\beta\gamma} \cdot \mathbf{K}_{\gamma\gamma} = \mu_\gamma \mathbf{K}_{\beta\beta} \cdot \mathbf{K}_{\gamma\beta}^T \quad (40)$$

These equations can also be rearranged into the following form [78]

$$\mathbf{V}_\beta = -\frac{1}{\mu_\beta} \mathbf{K}_{\beta\beta}^* \cdot (\nabla P_\beta - \rho_\beta \mathbf{g}) - \frac{1}{\mu_\gamma} \mathbf{K}_{\beta\gamma}^* \cdot (\nabla P_\gamma - \rho_\gamma \mathbf{g}) \quad (41)$$

$$\mathbf{V}_\gamma = -\frac{1}{\mu_\gamma} \mathbf{K}_{\gamma\gamma}^* \cdot (\nabla P_\gamma - \rho_\gamma \mathbf{g}) - \frac{1}{\mu_\beta} \mathbf{K}_{\gamma\beta}^* \cdot (\nabla P_\beta - \rho_\beta \mathbf{g}) \quad (42)$$

where the new multiphase permeability tensors are given by

$$\mathbf{K}_{\beta\beta}^* = [\mathbf{I} - \mathbf{K}_{\beta\gamma} \cdot \mathbf{K}_{\gamma\beta}]^{-1} \cdot \mathbf{K}_{\beta\beta} \quad (43)$$

$$\mathbf{K}_{\beta\gamma}^* = [\mathbf{I} - \mathbf{K}_{\beta\gamma} \cdot \mathbf{K}_{\gamma\beta}]^{-1} \cdot (\mathbf{K}_{\beta\gamma} \cdot \mathbf{K}_{\gamma\gamma}) \quad (44)$$

$$\mathbf{K}_{\gamma\beta}^* = [\mathbf{I} - \mathbf{K}_{\gamma\beta} \cdot \mathbf{K}_{\beta\gamma}]^{-1} \cdot (\mathbf{K}_{\gamma\beta} \cdot \mathbf{K}_{\beta\beta}) \quad (45)$$

$$\mathbf{K}_{\gamma\gamma}^* = [\mathbf{I} - \mathbf{K}_{\gamma\beta} \cdot \mathbf{K}_{\beta\gamma}]^{-1} \cdot \mathbf{K}_{\gamma\gamma} \quad (46)$$

The reciprocity relation Eq. 40 becomes

$$\mu_\beta \mathbf{K}_{\beta\gamma}^* = \mu_\gamma \mathbf{K}_{\gamma\beta}^{*T} \quad (47)$$

These equations are obtained following the upscaling framework described in Sec. a. Representations of the deviations have a structure similar (albeit extended to two phases) to Eq. 16, and closure problems are similar to the one described in a. The permeability tensors in Eqs. 39 or 42 can also be calculated from closure variables (see [26] and [78] for a detailed description).

[Figure 5 about here.]

The importance attributed to cross terms has been the subject of multiple controversies [76, 79, 77, 80, 81]. So far, these coupling terms have been discarded in applications related to petroleum engineering and many other fields. In low permeability rocks with a large variance of the pore sizes, this may be the consequence of the wetting phase having a tendency to flow in pores of small diameter while the non-wetting phase will flow in large pores. This phase repartition tends to minimize the interfacial area between the fluid phases, thus decreasing the importance of cross terms relative to the friction occurring at the solid/liquid interface. This may explain why measurements in media with a relatively low permeability have produced low values of the cross terms [80].

[Figure 6 about here.]

But the cross terms cannot be discarded in more structured media with high permeability. For instance, they can be computed for flow in capillaries of square [69, 77] or circular [82] sections. Assuming annular flow of two phases in a tube of radius R , as is illustrated Fig. 5, we can derive analytically the effective permeabilities. In the limit $\frac{\mu_\gamma}{\mu_\beta} \ll 1$ [83] we get

$$K_{\beta\beta} \approx K(1 - S_\gamma)^3 \quad (48)$$

$$K_{\beta\gamma} \approx \frac{\mu_g}{\mu_l} \frac{(1 - S_\gamma)^2}{S_\gamma} \quad (49)$$

$$K_{\gamma\gamma} \approx K S_\gamma^2 \quad (50)$$

$$K_{\gamma\beta} \approx \frac{S_\gamma}{1 - S_\gamma} \quad (51)$$

where $K = \frac{R^2}{8}$ is the tube permeability. Using the transformations provided by Eqs. 43 through 46, we have plotted the effective parameters in Fig. 6. Importantly, we see that the permeability cross

terms, $K_{\gamma\beta}^*$, are not negligible compared to the standard permeabilities. It was also emphasized recently that they account for a drag force necessary to explain the retention of water observed in a vertical column subject to an upward gas flow in the case of a high permeability medium [84, 85, 86, 34, 87, 83]. This effect is particularly important in chemical engineering or in nuclear safety (debris bed reflooding) applications. This question will be further discussed in Sec. a.

Macro-scale Dynamic Models

To get rid of the constraining assumptions of the previous Section, in particular the quasistatic assumption, several studies have proposed dynamic models which can be summarized as follows:

1. Dynamic effects can be captured by introducing additional non-linear dependencies in the capillary pressure and relative permeabilities, which are called pseudo-functions [88, 89, 90, 91, 92]. This approach is mostly used in petroleum engineering,
2. Several models account for dynamic effects induced by Darcy-scale heterogeneities and multi-zones [93], multi-zones [94], meniscus propagation [95],
3. The theory of irreversible thermodynamics yields models where the specific area of the fluid-fluid interface becomes a primary variable [69, 70, 71, 72],
4. Macro-scale versions of Cahn-Hilliard models have also been proposed [96].

This is beyond the scope of this review to provide a comprehensive literature survey of dynamic models. Here, our goal is essentially to emphasize that, besides differences in the mathematical structure, dynamic effects are often captured by introducing additional dependencies of the effective properties upon terms related to the flow velocity, gravity and transient effects. As an example, the equations from [93] read

$$\begin{aligned}
 \mathbf{V}_\beta = & -\frac{1}{\mu_\beta} \mathbf{K}_\beta^* \cdot (\nabla P_\beta - \rho_\beta \mathbf{g}) - \mathbf{u}_\beta^* \frac{\partial \varepsilon S_\beta}{\partial t} \\
 & - \mathbf{U}_\beta^* \cdot \nabla \frac{\partial \varepsilon S_\beta}{\partial t} - \frac{1}{\mu_\beta} \mathbf{M}_\beta^* : \nabla \nabla P_\beta \\
 & - \frac{1}{\mu_\beta} \Phi_\beta - \frac{1}{\mu_\beta} \mathbf{R}_\beta^* : \nabla \Phi_\beta
 \end{aligned} \tag{52}$$

for the β -phase macro-scale momentum equation and

$$p_c = \mathcal{F} \left(S_\beta, (\rho_\gamma - \rho_\beta) \mathbf{g}, \nabla P_\beta, \frac{\partial \varepsilon S_\beta}{\partial t}, \dots \right) \quad (53)$$

for the capillary pressure relationship. Here, several terms have been introduced to account for dynamic effects. Φ_β is a source of momentum due to the heterogeneities (see Eq. 2.28 in [93]), new effective properties (\mathbf{u}_β^* , \mathbf{U}_β^* , \mathbf{M}_β^* , \mathbf{R}_β^*) have been introduced and a gravity term is present to account for large Bond numbers. Similar theoretical results from [69, 71] are available with, besides an equation for the evolution of the interfacial specific area, a capillary pressure relationship with a relaxation term such as

$$P_\gamma - P_\beta = p_c - L_1 \frac{\partial \varepsilon S_\beta}{\partial t} \quad (54)$$

where L_1 is a phenomenological parameter.

Before going on to discuss inertia effects in the macro-scale models, we want to make a fundamental remark. Most models in the literature are based on quasistatic assumptions, which are not always satisfied by the micro-scale physics. Even if time appears explicitly in several dynamic models, the underlying assumption is that the motion of the interface is relatively slow, so that only spatial averaging is needed to derive macro-scale equations. Why then are these quasistatic models so popular and why are they satisfactory in many cases? We believe that there is more to this problem. One hypothesis is that, since meso-scale results have shown that a macro-scale representative state requires a large number of pores, some ergodicity between time and space averaging is at play. Hence, just averaging in space may be sufficient to smooth out high-frequency fluctuations of the pore-scale fields in time and space. If this hypothesis of ergodicity is incorrect, then this probably means that averaging must be performed in space and time: a great scientific challenge for future research.

Macro-scale Models with Inertial Effects

So far, the most complicated dynamic models (see Sec. a) have not been extended for flows with strong inertia effects. The simplest proposals to take these effects into account are based on

variants [97, 98] of a generalized Ergun's law, such as

$$0 = -\nabla P_\beta + \rho_\beta \mathbf{g} - \mu_\beta \frac{1}{K k_{r\beta}} \mathbf{V}_\beta - \frac{\rho_\beta}{\eta \eta_\beta} \|\mathbf{V}_\beta\| \mathbf{V}_\beta \quad (55)$$

where $k_{r\beta}$ is the relative permeability of the β -phase and where the Forchheimer term involves a relative passability η_β . A similar equation may be written for the γ -phase. The effective parameters, $k_{r\beta}$ and η_β , depend on the saturation and are often assigned the following forms

$$k_{r\beta} = (1 - S_\gamma)^n \quad ; \quad \eta_\beta = (1 - S_\gamma)^m \quad (56)$$

$$k_{r\gamma} = S_\gamma^p \quad ; \quad \eta_\gamma = S_\gamma^q \quad (57)$$

with different values for the exponents [99, 100, 101].

While this form may account for the increase in pressure drop due to inertial effects, it does not fully describe the drag between both phases and the resulting retention effects. Several models have been proposed to reproduce fluid-fluid interactions, for instance [86]⁴ proposed the following equations

$$0 = -\nabla P_\beta + \rho_\beta \mathbf{g} - \mu_\beta \frac{1}{K k_{r\beta}} \mathbf{V}_\beta - \frac{\rho_\beta}{\eta \eta_\beta} \|\mathbf{V}_\beta\| \mathbf{V}_\beta + \frac{\mathbf{F}_{\beta\gamma}^S}{S_\beta} \quad (58)$$

$$0 = -\nabla P_\gamma + \rho_\gamma \mathbf{g} - \mu_\beta \frac{1}{K k_{r\beta}} \mathbf{V}_\beta - \frac{\rho_\beta}{\eta \eta_\beta} \|\mathbf{V}_\beta\| \mathbf{V}_\beta - \frac{\mathbf{F}_{\beta\gamma}^S}{1 - S_\beta} \quad (59)$$

where the term $\mathbf{F}_{\beta\gamma}^S$ accounts for the interfacial interaction.

A generalized form of two-phase flow equations accounting for cross terms and inertia effects

⁴The original equations have been casted into a form suitable for comparison with generalized Darcy's law.

has been obtained theoretically through upscaling by [102] and reads

$$\begin{aligned} \mathbf{V}_\alpha = & -\frac{1}{\mu_\alpha} \mathbf{K}_\alpha \cdot (\nabla P_\alpha - \rho_\alpha \mathbf{g}) - \mathbf{F}_{\alpha\alpha} \cdot \mathbf{V}_\alpha \\ & + \mathbf{K}_{\alpha\kappa} \cdot \mathbf{V}_\kappa - \mathbf{F}_{\alpha\kappa} \cdot \mathbf{V}_\kappa \quad \alpha, \kappa = \beta, \gamma \quad \alpha \neq \kappa. \end{aligned} \quad (60)$$

The first two terms in the right-hand side of these equations correspond to a fully anisotropic generalization of the multiphase Ergun's law. The third term corresponds to viscous interactions, as already discussed in Sec. a, and the last term is a cross term mainly associated with the inertial correction. These models require the determination of several effective properties which depend non-linearly upon saturations and velocities, as well as on the viscosity ratio and geometrical features of the porous space. All these dependencies are not well understood today and determining these effective properties from Direct Numerical Simulations or experiments remains an open problem and a challenging task.

To illustrate the capabilities of the various models, let us consider two-phase flow in a vertical column of high permeability (and hence small capillary effects). Initially, the porous medium is saturated by a liquid phase, β , and an upward flow of a gas phase, γ , is imposed. The fluid phase will be progressively ejected by the top of the column until the situation reaches steady-state and $\mathbf{V}_\beta = 0$. Using the more general form Eq. 60, we have that

$$0 = -\frac{1}{\mu_\beta} K_\beta \left(\frac{\partial P_\beta}{\partial z} - \rho_\beta \mathbf{g} \cdot \mathbf{e}_z \right) + (K_{\beta\gamma} - F_{\beta\gamma}) V_\gamma \quad (61)$$

On the other hand, using only the classical generalized Darcy's laws, i.e., $(K_{\beta\gamma} - F_{\beta\gamma}) = 0$, one gets

$$\frac{\partial P_\beta}{\partial z} = \rho_\beta \mathbf{g} \cdot \mathbf{e}_z \quad (62)$$

The result of the generalized Darcy's laws *does not agree* with experimental data [103, 87]. This is illustrated in Fig. 7, which represents the data obtained from experiments through a cylindrical porous column by [104, 83], as well as theoretical results. In these experiments, the column was

initially saturated by water (β -phase), then gas (γ -phase) was injected from below. Liquid flowed out of the column from the top until a quasi-steady macro-scale situation was obtained. The figure shows the pressure gradient normalized by the liquid hydrostatic pressure gradient versus the gas velocity, for a liquid average velocity equal to zero. The simple generalized Darcy's law models with Ergun's type inertia term (Eq. 62), as proposed by [105], [106] or [101], yield completely erroneous results. Below a critical velocity, the fluid is lifted by the gas and has a decreasing apparent weight. This corresponds to the viscous interactions, which in the model are captured by the term involving $K_{\beta\gamma}$. When the velocity is further increased, inertial effects, as taken into account in Eq. 61 by the extra term involving $F_{\beta\gamma}$, tend to reduce the lift and increase the apparent weight.

In summary, keeping the extra terms in Eq. 61 allows to account for liquid retention due to the drag force imposed on the liquid by the upward flow for a large range of Reynolds number. Various expressions have been proposed in the literature for the effective parameters [86, 107, 83] and their application to [87] experiments are reported in Figs. 7 and 8. High non-linearity, lack of data and the large number of parameters that needs to be determined lead to strong difficulties in the identification procedure. This may explain the discrepancy observed between data and predictions [108, 109, 87] as is shown in Figs 7 and 8 adapted from [87]. Further research is therefore necessary to better parametrize the models.

[Figure 7 about here.]

[Figure 8 about here.]

Two-Phase Flows: Special Models

In this section, we review two-phase flow models that have been proposed to reproduce specific mechanisms observed at high capillary and Bond numbers. In such cases, the time and length-scale constraints which are necessary to develop macro-scale two-phase flow models are not fulfilled. Therefore, specific treatments and assumptions are needed. Two types of models have been proposed and are the subject of current research. They are briefly presented below.

Models with a Splitting of Phase

Structured packings have been extensively used in the past decades in absorption and distillation columns or chemical reactors. They are often made of assemblies of corrugated metal sheets, alternating the orientation from one sheet to another, thus creating a porous medium having the honeycomb structure illustrated Fig. 9. The resulting material has a relatively high surface area and small pressure drops. The characteristic length for the pores is several millimeters (sometimes up to the centimeter), thus pore-scale flow in such devices is sensitive to effects of gravity and inertia.

[Figure 9 about here.]

Further, the alternating directions of the structure may create preferential flowpaths which are followed by only a portion of the fluid. For such geometries, a single macro-scale equation describing the liquid phase flow is often not very accurate, as it fails to account for the bimodal distribution of flow angles. Models with a liquid phase decomposed into two pseudo-phases, i.e., one macro-scale equation for the gas phase but two macro-scale equations for the liquid, have been proposed to handle such cases [110, 111, 112, 113]. The result is a set of balance equations for the gas phase (a single effective phase is enough in the context of structured packings), γ , and two sets of balance equations, one for liquid phase part 1, β_1 , and one for liquid phase part 2, β_2 . For instance, the three mass balance equations read

$$\varepsilon \frac{\partial S_\gamma}{\partial t} + \nabla \cdot \mathbf{V}_\gamma = 0, \quad (63)$$

$$\varepsilon \frac{\partial S_{\beta_1}}{\partial t} + \nabla \cdot \mathbf{V}_{\beta_1} = \dot{m}, \quad (64)$$

$$\varepsilon \frac{\partial S_{\beta_2}}{\partial t} + \nabla \cdot \mathbf{V}_{\beta_2} = -\dot{m}. \quad (65)$$

where \dot{m} is the mass exchange term which must be modeled in terms of the three "phases" saturations, pressures and velocities.

While there were attempts to develop these models through volume averaging, part of the resulting models are still heuristic. In particular, the description of the exchange of mass (and

momentum) between the two macro-scale liquid phases remains an open problem. To illustrate this, let us consider the spreading of a *single* jet impinging such a porous medium as described by these models (Fig. 10 and Fig. 11 taken from [113]). We see in Fig. 10 that the impinging jet tends to be distributed in two jets along the two directions of the corrugated sheets. On the other hand, exchange between the phases, as expressed by the term m in Eqs. 64 and 65, tends to smear out this double jet structure. Depending on the intensity of the exchange term, the two liquid phases show a distinct shape with two separate jets when there is barely no exchange, or a more classical solution when the exchange is strong. These two shapes have been observed experimentally [111, 114]. The results obtained by [114] are presented in Fig. 11a. This figure is a plot of $S_{\beta_1} + S_{\beta_2}$ at a given cross-section of the experimental column. It clearly shows the anisotropic spreading of the jet due to the peculiar geometry of the structured medium. Fig. 11b to Fig. 11h show predictions obtained in [115], for increasing values of the exchange term. These results demonstrate that such models have the potential for representing experimental data. However, the accurate determination of the effective properties needed in such models requires further investigations.

[Figure 10 about here.]

[Figure 11 about here.]

Dynamic meso-scale and Hybrid models

In porous media with low capillarity effects, the liquid moves by a series of different mechanisms:

- films developing over the grain surfaces,
- bridges forming between films when close to contact points,
- bulging films due to either instabilities or the effect of high Bond numbers.

This flow complexity is illustrated by the CFD results from [116], which are presented in Fig. 12. The results show the spreading of a liquid film from a jet impacting the north pole of the top sphere in a vertical stack. The liquid then spreads as a film, reaches the contact point where films develop

on the adjacent spheres, and goes on to the next sphere. As a consequence of the diversity of mechanisms at play, several flow regimes may develop as illustrated, for instance, in [117], [118], [119] and [120]. Such regimes can be easily observed when studying the quasi-2D flow of a liquid in a bundle of cylinders as illustrated in Fig. 13 (left) taken from [121]. The porous medium is a micromodel with pillars, and the photograph shows the distribution of phases resulting from a jet impacting the upper part of the cylinder in the middle. The jet spreads laterally because of bulging film contacting adjacent pillars, a mechanism that cannot be described easily at the macro-scale by capillary diffusion effect embedded in the classical Generalized Darcy's laws. In addition, the length-scale constraints (Eq. 1) necessary to develop a macro-scale theory are not satisfied.

The flow complexity can be captured by direct numerical modeling [122] as illustrated in Fig. 13 (right) where the flow between the cylinders is obtained using a Volume of Fluids method [121]. Two limitations arise for a direct application of CFD to complex systems. First, it is difficult to obtain deterministic predictions since many of the mechanisms involved are subject to unpredictability (e.g. instabilities, sensitivity to small geometrical features). Second, it is very difficult to get accurate, converged and stable numerical solutions, even for a limited number of pores. Nowadays, accurate calculations for a large amount of pores, especially in 3D, is beyond the capabilities of modern computers. Indeed, even for a porous medium with a correlation length of the order of the grain size, the phase repartition pattern develops over dozens of pores. In such cases, we are faced with the following difficulties:

1. the complexity of pore-scale mechanisms and the broad range of time and spatial characteristic scales, make the development of a macro-scale model very difficult to achieve,
2. Direct Numerical Solution (DNS) is equally very difficult to carry on because of the number of pores involved.

[Figure 12 about here.]

[Figure 13 about here.]

As discussed in Sec. a, it is often convenient to use a simplified meso-scale description of the porous medium as a pore network model. This is particularly true when complex percolation mechanisms are encountered. Rules describing the flow between and within nodes must be introduced. This is relatively straightforward for classical percolation problems (Poiseuille like pressure drop for describing the flow between nodes and quasistatic capillary effects [73, 123]), but these rules must be adapted for dynamic cases. Dynamic rules may be introduced directly in the network model [120, 124, 125, 40, 126] under the form of dynamic pressure drop relationships or even a stochastic distribution of the phase entering a node into the adjacent links. These rules can be obtained heuristically, experimentally or with the help of localized (i.e., over a small number of pores) direct numerical simulations. In that last case, meso-scale simulations are coupled with pore-scale simulations, so that we often refer to such models as *hybrid models*. The idea of such approaches is to couple the pore-network description with local pore-scale simulations carried out with, for instance, a Volume Of Fluid numerical model. The local VOF simulations provides the dynamic rules necessary to advance the fluid flow in the pore network model. This hybrid modeling is schematically illustrated Fig. 14.

As an illustration of the meso-scale approach, Fig. 15 represents the saturation and pressure field obtained by [126] for gas–liquid trickle flows inside fixed beds of spherical particles. The geometry is first obtained using X-ray micro-tomography. Then the flow in the throats between pores is described using the results for the annular two-phase flow in tubes described in Sec. a, i.e., the model with cross-terms. Finally, the flow distribution between pores and throats is obtained by solving mass and momentum balance equations. While results are promising, further work is needed to make these models operational in engineering practice. It must also be reminded that meso-scale models need more computational resources than macro-scale representations. Therefore, efforts to obtain more dynamic purely macro-scale models must also continue.

[Figure 14 about here.]

[Figure 15 about here.]

Conclusions

In this paper, we have reviewed one- and two-phase flows in highly permeable porous media, with an emphasis on macro-scale modeling at high Reynolds, Capillary and Bond numbers.

For one-phase flow, we have shown that moderate inertial effects can be captured by modifications of Darcy's law. For large Reynolds numbers, however, when time fluctuations becomes important, there are still many unanswered questions regarding the time averaging procedure, the form of the drag, the localization of the flow structures and the development of fully macro-scale turbulent models. For two-phase flows in the creeping limit, we have shown that the generalized Darcy's law can be extended to account for couplings between the two phases via cross terms. In the case high Reynolds numbers, several models were proposed that can be classified in two categories. First, there are extensions of Ergun's one-phase model to the two-phase flow case, with relative permeabilities and passabilities as the main effective parameters. Second, several models with additional interaction terms have been obtained heuristically or via upscaling procedures. These models reproduce the experimental results available with relatively good accuracy. However, it is clear from the comparison between predictions and experimental data that additional work should be done to yield better estimates of the various non-linear expressions for the effective parameters used in these models.

This review also shows that many problems remain largely open for two-phase flow at large Bond and capillary numbers. For this case, classical quasistatic formulations seem to work in the situation where, in theory, they should not, as dynamic effects are important. An hypothesis is that of a time/space ergodicity, which would eliminate the need for temporal averaging, although this needs to be explored more thoroughly. We have also shown that hybrid models have been proposed in the literature, which couple solutions of the problem at different scales. Such formulations represent an interesting alternative to macro-scale models with the potential to be more accurate and capture more dynamic phenomena. Because of their computational cost, they are often limited and cannot supplant macro-scale formulations, but can this change with the advent of high performance computing?

There are also many open problems that are specific to given porous structures, such as those inducing bi-structured flows with almost independent behaviors of different portions of the liquid phase. Models with a splitting of the liquid (or gas) flow into two macro-scale fluids have shown their ability to reproduce results qualitatively but, once again, much work should be devoted to the validation of the mathematical structure of such models and the estimation of the relevant effective transport properties.

Appendix: Closure problem for Darcy's law

There are several possible versions of the closure problems. The one corresponding to the mapping given by Eqs. 16 is described by the following PDEs

$$\nabla \cdot \mathbf{B} = 0 \quad (66)$$

$$-\nabla \mathbf{b} + \nabla^2 \mathbf{B} = \varepsilon_\beta^{-1} \frac{1}{V} \int_{A_{\beta\sigma}} \mathbf{n}_{\beta\sigma} \cdot (-\mathbf{I} \mathbf{b} + \nabla \mathbf{B}) dA \quad (67)$$

$$\mathbf{B} = -\mathbf{I} \quad \text{at } A_{\beta\sigma} , \quad (68)$$

$$\langle \mathbf{b} \rangle^\beta = 0 \quad (69)$$

$$\mathbf{b}(\mathbf{r} + \mathbf{l}_i) = \mathbf{b}(\mathbf{r}) \quad \mathbf{B}(\mathbf{r} + \mathbf{l}_i) = \mathbf{B}(\mathbf{r}) \quad (70)$$

The mapping tensor \mathbf{B} has the following property

$$\langle \mathbf{B} \rangle^\beta = 0 \quad (71)$$

which, together with Eq. 69, ensure that the averages of the deviations are zero.

Other forms can be developed to eliminate the integro-differential terms in the closure problem, see [78] for such transformations. This generally leads to problems that are similar to a Stokes problem over a periodic unit cell with a constant source term (the gradient of the averaged pressure). Such a form can readily be used to calculate the permeability tensor from a classical CFD software.

The use of periodicity conditions is correct for periodic systems. This approximation, however, may pose problems for systems which are not truly periodic. This point is not discussed further in this paper and the reader may look at the literature on the subject, for instance in [127], for indications on how to overcome this difficulty.

Nomenclature

β_i refers to the split β -phase

\dot{m} mass exchange term

η passability

η_β relative passability

γ_β β -phase indicator

$\langle \psi_\beta \rangle$ β -phase average

$\langle \psi_\beta \rangle^\beta$ β -phase intrinsic average

b, B mapping variables

$\mathbf{F}_{\alpha\kappa}^S$ inertia multiphase effective properties

$\mathbf{F}_{\beta\gamma}^S$ interfacial interaction

K intrinsic permeability tensor

$\mathbf{K}_{\alpha\kappa}$ cross term

$\mathbf{K}_{\alpha\kappa}^*$ modified multiphase permeability tensor

M Navier tensor

$\mathbf{n}_{\beta\sigma}$ normal to $A_{\beta\sigma}$

U_β	β -phase intrinsic velocity
$\mathbf{u}_\beta^*, \mathbf{U}_\beta^*, \mathbf{M}_\beta^*, \mathbf{R}_\beta^*$	new effective properties, Eq. 52
\mathbf{V}_β	β -phase filtration velocity
\mathbf{v}_β	β -phase velocity
\mathbf{v}_s	velocity on effective surface
\mathbf{x}	current point
\mathbf{y}	position relative to the centroid
μ_β	β -phase dynamic viscosity
ψ_β	β -phase variable
ρ_β	β -phase density
σ	interfacial tension
$\tilde{\mathbf{v}}_\beta$	velocity deviation
\tilde{p}_β	pressure deviation
ε	porosity
ε_β	β -phase volume fraction
$a_{\beta\gamma}$	specific interfacial area
$A_{\beta\sigma}$	interface between the fluid and solid phases
d	particle diameter
F	inertia term
g	gravity acceleration

h_η	passability correction factor
h_k	permeability correction factor
$H_{\beta\gamma}$	interface curvature
$k_{r\alpha}$	α -phase relative permeability
L	large-scale characteristic length
L_1	phenomenological parameter
l_σ	pore-scale characteristic length
l_p	pore-scale characteristic length
p_c	capillary pressure
P_β	intrinsic phase average pressure viscosity
p_β	β -phase pressure
r_0	averaging volume characteristic length
S_β	β -phase saturation
U_r	reference velocity
V	averaging volume
V_β	β -phase volume
Bo	Bond number
Ca	capillary number
Re	Reynolds number

*

References

- [1] Darcy, H. *Fontaines Publiques de la Ville de Dijon*. Dalmont, Paris, 1856.
- [2] Muskat, M. *The Flow of Homogeneous Fluids Through Porous Media*. International Series in Physics. York The Mapple Press Company, 1946.
- [3] Bourgeat, A., Quintard, M. and Whitaker, S. Eléments de Comparaison entre la Méthode d'Homogénéisation et la Méthode de Prise de Moyenne avec Fermeture. *Compte Rendu de l'Académie des Sciences de Paris*, vol. 306, série II, pp. 463–466, 1988.
- [4] Wood, B., Cherblanc, F., Quintard, M. and Whitaker, S. Volume Averaging for Determining the Effective Dispersion Tensor: Closure Using Periodic Unit Cells and Comparison with Ensemble Averaging. *Water Resources Research*, vol. 39, no. 6, pp. 1154–1173, 2003.
- [5] Davit, Y., Bell, C. G., Byrne, H. M., Chapman, L. A., Kimpton, L. S., Lang, G. E., Leonard, K. H., Oliver, J. M., Pearson, N. C., Shipley, R. J., Waters, S. L., Whiteley, J. P., Wood, B. D. and Quintard, M. Homogenization via Formal Multiscale Asymptotics and Volume Averaging: How do the Two Techniques Compare? *Advances in Water Resources*, vol. 62, pp. 178–206, 2013.
- [6] Davit, Y. and Quintard, M. *Theoretical Analysis of Transport in Porous Media: Multi-Equation and Hybrid Models for a Generic Transport Problem with Non-Linear Source Terms in Handbook of Porous Media*, chapter 7. Ed. by K. Vafai, Taylor & Francis, 2015.
- [7] Marle, C. M. Application de la Méthode de la Thermodynamique des Processus Irréversible à l'Écoulement d'un Fluide à Travers un Milieu Poreux. *RILEM Bulletin*, vol. 29, pp. 1066–1071, 1965.
- [8] Marle, C. M. On Macroscopic Equations Governing Multiphase Flow with Diffusion and Chemical Reactions in Porous Media. *International Journal of Engineering Science*, vol. 20, no. 5, pp. 643–662, 1982.

- [9] Whitaker, S. Diffusion and Dispersion in Porous Media. *AICHE Journal*, vol. 13, pp. 420–427, 1967.
- [10] Whitaker, S. *The Method of Volume Averaging*. Kluwer Academic Publishers, Dordrecht, The Netherlands, 1999.
- [11] Gray, W. G. and Hassanizadeh, S. M. Macroscale Continuum Mechanics for Multiphase Porous-Media Flow Including Phases, Interfaces, Common Lines and Common Points. *Advances in Water Resources*, vol. 21, pp. 261–281, 1998.
- [12] Bensoussan, J., Lions, L. and Papanicolaou, G. *Asymptotic Analysis for Periodic Structures*. North-Holland, Amsterdam, 1978.
- [13] Tartar, L. *The General Theory of Homogenization: A Personalized Introduction*. Lecture Notes of the Unione Matematica Italiana. Springer, 2009.
- [14] Auriault, J.-L., Boutin, C. and Geindreau, C. *Homogenization of Coupled Phenomena in Heterogeneous Media*, volume vol. 149. John Wiley & Sons, 2010.
- [15] Matheron, G. *Les Variables Régionalisées et leur Estimation : une Application de la Théorie des Fonctions Aléatoires aux Sciences de la Nature*. Masson, Paris, 1965.
- [16] Gelhar, L. W. and Collins, M. A. General Analysis of Longitudinal Dispersion in Nonuniform Flow. *Water Resources Research*, vol. 7, no. 6, pp. 1511–1521, 1971.
- [17] Dagan, G. *Flow and Transport in Porous Formations*. Springer-Verlag, Berlin, 1989.
- [18] Quintard, M. and Whitaker, S. Transport in Ordered and Disordered Porous Media 1: the Cellular Average and the Use of Weighting Functions. *Transport in Porous Media*, vol. 14, pp. 163–177, 1994.
- [19] Quintard, M. and Whitaker, S. Transport in Ordered and Disordered Porous Media 2: Generalized Volume Averaging. *Transport in Porous Media*, vol. 14, pp. 179–206, 1994.

- [20] Quintard, M. and Whitaker, S. Transport in Ordered and Disordered Porous Media 3: Closure and Comparison Between Theory and Experiment. *Transport in Porous Media*, vol. 15, pp. 31–49, 1994.
- [21] Quintard, M. and Whitaker, S. Transport in Ordered and Disordered Porous Media 4: Computer Generated Porous Media. *Transport in Porous Media*, vol. 15, pp. 51–70, 1994.
- [22] Quintard, M. and Whitaker, S. Transport in Ordered and Disordered Porous Media 5: Geometrical Results for Two-Dimensional Systems. *Transport in Porous Media*, vol. 15, pp. 183–196, 1994.
- [23] Davit, Y. and Quintard, M. Technical Notes on Volume Averaging in Porous Media I: How is Spatial Averaging Defined for Periodic and Quasiperiodic Structures? *Submitted to Transport in Porous Media*, 2017.
- [24] Chauveteau, G. and Thirriot, C. Régimes d'Écoulement en Milieu Poreux et Limite à la Loi de Darcy. *La Houille Blanche*, vol. 2, pp. 141–148, 1967.
- [25] Sanchez-Palencia, E. On the Asymptotics of the Fluid Flow Past an Array of Fixed Obstacles. *International Journal of Engineering Science*, vol. 20, no. 12, pp. 1291–1301, 1982.
- [26] Whitaker, S. Flow in Porous Media 1: a Theoretical Derivation of Darcy's Law. *Transport in Porous Media*, vol. 1, pp. 3–25, 1986.
- [27] Wodié, J. and Levy, T. Correction non Linéaire à la Loi de Darcy. *Compte Rendu de l'Académie des Sciences de Paris*, vol. 312, série II, pp. 157–161, 1991.
- [28] Mei, C. and Auriault, J. The Effect of Weak Inertia on Flow Through a Porous Medium. *Journal of Fluid Mechanics*, vol. 222, pp. 647–663, 1991.
- [29] Firdaouss, M., Guermond, J. and Le Quéré, P. Non Linear Corrections to Darcy's Law at Low Reynolds Numbers. *Journal of Fluid Mechanics*, vol. 343, pp. 331–350, 1997.

- [30] Skjetne, E. and Auriault, J. High Velocity Laminar and Turbulent Flow in Porous Media. *Transport in Porous Media*, vol. 36, pp. 131–147, 1999.
- [31] Lasseux, D., Abbasian, A. and Ahmadi, A. On the Stationary Macroscopic Inertial Effects for One-Phase Flow in Ordered and Disordered Porous Media. *Physics of Fluids*, vol. 23, 2011.
- [32] Pasquier, S., Quintard, M. and Davit, Y. Modeling Flow in Porous Media With Rough Surfaces: Effective Slip Boundary Conditions and Application to Structured Packings. *Chemical Engineering Science*, vol. 165, pp. 131 – 146, 2017.
- [33] Forchheimer, P. Wasserbewegung Durch Boden. *Zeitschrift Ver. Deutsch Ing.*, vol. 45, pp. 1782–1788, 1901.
- [34] Yazdchi, K. and Luding, S. Toward Unified Drag Laws for Inertial Flows Through Fibrous Media. *Chemical Engineering Journal*, vol. 207, pp. 35–48, 2012.
- [35] Ergun, S. Fluid Flow Through Packed Columns. *Chemical Engineering Progress*, vol. 48, no. 2, pp. 89–94, 1952.
- [36] Lage, J., Antohe, B. and Nield, D. Two Types of Non-Linear Pressure-Drop Versus Flow-Rate Relation Observed for Saturated Porous Media. *Transactions of the ASME*, vol. 119, pp. 700–706, 1997.
- [37] Clavier, R., Chikhi, N., Fichot, F. and Quintard, M. Experimental Investigation on Single-Phase Pressure Losses in Nuclear Debris Beds: Identification of Flow Regimes and Effective Diameter. *Nuclear Engineering and Design*, vol. 292, pp. 222–236, 2015.
- [38] MacDonald, I., El-Sayed, M., Mow, K. and Dullien, F. Flow Through Porous Media - the Ergun Equation Revisited. *Industrial and Engineering Chemistry Fundamentals*, vol. 18, pp. 199–208, 1979.

- [39] Li, L. and Ma, W. Experimental Study on the Effective Particle Diameter of a Packed Bed With Non-Spherical Particles. *Transport in Porous Media*, vol. 89, pp. 35–48, 2011.
- [40] Larachi, F., Hannaoui, R., Horgue, P., Augier, F., Haroun, Y., Youssef, S., Rosenberg, E., Prat, M. and Quintard, M. X-Ray Micro-Tomography and Pore Network Modeling of Single-Phase Fixed-Bed Reactors. *Chemical Engineering Journal*, vol. 240, pp. 290–306, 2014.
- [41] Vafai, K. and Tien, C. L. Boundary and Inertia Effects on Flow and Heat Transfer in Porous Media. *International Journal of Heat and Mass Transfer*, 24, pp. 195–203, 1981.
- [42] Phanikumar, M. S. and Mahajan, R. L. Non-Darcy Natural Convection in High Porosity Metal Foams. *International Journal of Heat and Mass Transfer*, 45, no. 18, pp. 3781–3793, 2002.
- [43] Fichot, F., Duval, F., Trégourès, N., Béchaud, C. and Quintard, M. The Impact of Thermal Non-equilibrium and Large-Scale 2D/3D Effects on Debris Bed Reflooding and Coolability. *Nuclear Engineering and Design*, 236, no. 19, pp. 2144–2163, 2006.
- [44] Beale, S. B. A Simple, Effective Viscosity Formulation for Turbulent Flow and Heat Transfer in Compact Heat Exchangers. *Heat Transfer Engineering*, 33, no. 1, pp. 4–11, 2012.
- [45] Bousri, A., Nebbali, R., Bennacer, R., Bouhadef, K. and Beji, H. Numerical Investigation of Forced Convection Nonequilibrium Effects on Heat and Mass Transfer in Porous Media. *Heat Transfer Engineering*, 38, no. 1, pp. 122–136, 2017.
- [46] Soulaine, C. and Quintard, M. On the Use of Darcy-Forchheimer Like Model for a Macro-Scale Description of Turbulence in Porous Media and Its Application to Structured Packings. *International Journal of Heat and Mass Transfer*, vol. 74, pp. 88–100, 2014.
- [47] Jin, Y., Uth, M.-F., Kuznetsov, A. and Herwig, H. Numerical Investigation of the Possibility

- of Macroscopic Turbulence in Porous Media: A Direct Numerical Simulation Study. *Journal of Fluid Mechanics*, vol. 766, pp. 76–103, 2015.
- [48] Chandesris, M., D’Hueppe, A., Mathieu, B., Jamet, D. and Goyeau, B. Direct Numerical Simulation of Turbulent Heat Transfer in a Fluid-Porous Domain. *Physics of Fluids*, vol. 25, no. 12, pp. 125110, 2013.
- [49] Agnaou, M., Lasseux, D. and Ahmadi, A. From Steady to Unsteady Laminar Flow in Model Porous Structures: An Investigation of the First Hopf Bifurcation. *Computers & Fluids*, vol. 136, pp. 67–82, 2016.
- [50] de Lemos, M. *Turbulence in Porous Media: Modeling and Applications*. Elsevier Science Ltd, 2006.
- [51] Antohe, B. and Lage, J. A General Two-Equation Macroscopic Turbulence Model for Incompressible Flow in Porous Media. *International Journal of Heat and Mass Transfer*, vol. 40, no. 13, pp. 3013–3024, 1997.
- [52] Getachew, D., Minkowycz, W. and Lage, J. A Modified Form of the κ - ε Model for Turbulent Flows of an Incompressible Fluid in Porous Media. *International Journal of Heat and Mass Transfer*, 43, no. 16, pp. 2909–2915, 2000.
- [53] Kuwahara, F., Kameyama, Y., Yamashita, S. and Nakayama, A. Numerical Model of Turbulent Flow in Porous Media Using a Spatially Periodic Array. *Journal of Porous Media*, vol. 1, pp. 47–55, 1998.
- [54] Nakayama, A. and Kuwahara, F. A Macroscopic Turbulence Model for Flow in a Porous Medium. *Journal of Fluids Engineering*, vol. 121, no. 2, pp. 427–433, 1999.
- [55] Pedras, M. H. and de Lemos, M. J. Macroscopic Turbulence Modeling For Incompressible Flow Through Undeformable Porous Media. *International Journal of Heat and Mass Transfer*, vol. 44, no. 6, pp. 1081–1093, 2001.

- [56] Achdou, Y., Pironneau, O. and Valentin, F. Effective Boundary Conditions for Laminar Flows Over Periodic Rough Boundaries. *Journal of Computational Physics*, vol. 147, pp. 187–218, 1998.
- [57] Veran, S., Aspa, Y. and Quintard, M. Effective Boundary Conditions for Rough Reactive Walls in Laminar Boundary Layers. *International Journal of Heat and Mass Transfer*, vol. 52, pp. 3712–3725, 2009.
- [58] Introïni, C., Quintard, M. and Duval, F. Effective Surface Modeling for Momentum and Heat Transfer Over Rough Surfaces: Application to a Natural Convection Problem. *International Journal of Heat and Mass Transfer*, vol. 54, pp. 3622–3641, 2011.
- [59] Lenormand, R., Touboul, E. and Zarcone, C. Numerical Models and Experiments on Immiscible Displacements in Porous Media. *Journal of Fluid Mechanics*, vol. 189, pp. 165–187, 1988.
- [60] Zhao, B., MacMinn, C. and Juanes, R. Wettability Control on Multiphase Flow in Patterned Microfluidics. *Proceedings of National Academy of Sciences U.S.A.*, vol. 111, no. 37, pp. 10251–10256, 2016.
- [61] Haines, W. B. Studies in the Physical Properties of Soil. v. the Hysteresis Effect in Capillary Properties, and the Modes of Moisture Distribution Associated Therewith. *The Journal of Agricultural Science*, vol. 20, no. 1, pp. 97–116, 1930.
- [62] Berg, S., Ott, H., Klapp, S. A., Schwing, A., Neiteler, R., Brussee, N., Makurat, A., Leu, L., Enzmann, F., Schwarz, J.-O. *et al.* Real-Time 3D Imaging of Haines Jumps in Porous Media Flow. *Proceedings of the National Academy of Sciences*, vol. 110, no. 10, pp. 3755–3759, 2013.
- [63] Ransohoff, T., Gauglitz, P. and Radke, C. Snap-Off of Gas Bubbles in Smoothly Constricted Noncircular Capillaries. *AIChE Journal*, vol. 33, no. 5, pp. 753–765, 1987.

- [64] Kovscek, A. and Radke, C. Gas Bubble Snap-Off Under Pressure-Driven Flow in Constricted Noncircular Capillaries. *Colloids and Surfaces A: Physicochemical and Engineering Aspects*, vol. 117, no. 1, pp. 55–76, 1996.
- [65] Legait, B. Laminar Flow of Two Phases Through a Capillary Tube with Variable Square Cross-Section. *Journal of Colloid and Interface Science*, vol. 96, no. 1, pp. 28–38, 1983.
- [66] Chatzis, I., Morrow, N. R. and Lim, H. T. Magnitude and Detailed Structure of Residual Oil Saturation. *Society of Petroleum Engineers Journal*, vol. 23, no. 2, pp. 311–326, 1983.
- [67] Schlüter, S., Berg, S., Rücker, M., Armstrong, R., Vogel, H.-J., Hilfer, R. and Wildenschild, D. Pore-Scale Displacement Mechanisms as a Source of Hysteresis for Two-Phase Flow in Porous Media. *Water Resources Research*, vol. 52, no. 3, pp. 2194–2205, 2016.
- [68] Morrow, N. R. and Harris, C. C. Capillary Equilibrium in Porous Materials. *Society of Petroleum Engineers Journal*, vol. 5, no. 1, pp. 15–24, 1965.
- [69] Kalaydjian, F. A Macroscopic Description of Multiphase Flow in Porous Media Involving Spacetime Evolution of Fluid/Fluid Interface. *Transport in Porous Media*, vol. 2, no. 6, pp. 537–552, 1987.
- [70] Gray, W. G. and Hassanizadeh, S. M. Unsaturated Flow Theory Including Interfacial Phenomena. *Water Resources Research*, vol. 27, no. 8, pp. 1855–1863, 1991.
- [71] Hassanizadeh, M. and Gray, W. G. Toward an Improved Description of the Physics of Two-Phase Flow. *Advances in Water Resources*, vol. 16, no. 1, pp. 53–67, 1993.
- [72] Reeves, P. C. and Celia, M. A. A Functional Relationship Between Capillary Pressure, Saturation, and Interfacial Area as Revealed by a Pore-Scale Network Model. *Water Resources Research*, vol. 32, no. 8, pp. 2345–2358, 1996.
- [73] Dullien, F. *Porous Media: Fluid Transport and Pore Structure*. Academic Press, 1979.

- [74] Lenormand, R. Liquids in Porous Media. *Journal of Physics: Condensed Matter*, vol. 2, no. S, pp. SA79, 1990.
- [75] Auriault, J.-L. Nonsaturated Deformable Porous Media: Quasistatics. *Transport in Porous Media*, vol. 2, pp. 45–64, 1987.
- [76] Rose, W. Measuring Transport Coefficients Necessary for the Description of Coupled Two-Phase Flow of Immiscible Fluids in Porous Media. *Transport in Porous Media*, vol. 3, pp. 163–171, 1988.
- [77] Kalaydjian, F. Origin and Quantification of Coupling Between Relative Permeabilities for Two-Phase Flows in Porous Media. *Transport in Porous Media*, vol. 5, pp. 215–229, 1990.
- [78] Lasseux, D., Quintard, M. and Whitaker, S. Determination of Permeability Tensors for Two-Phase Flow in Homogeneous Porous Media: Theory. *Transport in Porous Media*, vol. 24, pp. 107–137, 1996.
- [79] Bourbiaux, B. J. and Kalaydjian, F. J. Experimental Study of Cocurrent and Countercurrent Flows in Natural Porous Media. *SPE Reservoir Engineering*, vol. 5, pp. 361–368, 1990.
- [80] Zarcone, C. and Lenormand, R. Détermination Expérimentale du Couplage Visqueux dans les Écoulements Diphasiques en Milieu Poreux. *Comptes Rendus de L'Académie des Sciences Paris Série II*, vol. 318, pp. 1429–1435, 1994.
- [81] Rose, W. Myths About Later-Day Extensions of Darcy's Law. *Journal of Petroleum Science and Engineering*, vol. 26, no. 1-4, pp. 187–198, 2000.
- [82] Bacri, J. C., Chaouche, M. and Salin, D. Modèle Simple de Perméabilités Relatives Croisées. *Comptes Rendus de L'Académie des Sciences Paris Série II*, vol. 311, pp. 591–597, 1990.
- [83] Clavier, R., Chikhi, N., Fichot, F. and Quintard, M. Modeling of Inertial Multi-Phase Flows through High Permeability Porous Media: Friction Closure Laws. *International Journal of Multiphase Flow*, vol. 91, pp. 243–261, 2017.

- [84] Dhir, V. and Barleon, L. Dryout Heat-flux in a Bottom-heated Porous Layer. In *Transactions of the American Nuclear Society*, volume vol. 38, 385–386. 1981.
- [85] Lipinski, R. J. Model for Boiling and Dryout in Particle Beds.[LMFBR]. Technical report, Sandia National Labs., Albuquerque, NM (USA), 1982.
- [86] Schulenberg, T. and Müller, U. An Improved Model for Two-Phase Flow Through Beds of Coarse Particles. *International Journal of Multiphase Flow*, vol. 13, pp. 87–97, 1987.
- [87] Chikhi, N., Clavier, R., Laurent, J.-P., Fichot, F. and Quintard, M. Pressure Drop and Average Void Fraction Measurements for Two-Phase Flow Through Highly Permeable Porous Media. *Annals of Nuclear Energy*, vol. 94, pp. 422–432, 2016.
- [88] Hearn, C. L. Simulation of Stratified Waterflooding by Pseudo Relative Permeability Curves. In *Paper SPE 2929 Presented at the 45th Annual Fall Meeting of the Society of Petroleum Engineers, Houston*. 1970.
- [89] Kyte, J. R., Berry, D. *et al.* New Pseudo Functions to Control Numerical Dispersion. *Society of Petroleum Engineers Journal*, vol. 15, no. 4, pp. 269–276, 1975.
- [90] Barker, J. and Thibeau, S. A Critical Review of the Use of Pseudorelative Permeabilities for Upscaling. *SPE Reservoir Engineering*, vol. 12, pp. 138–143, 1997.
- [91] Quintard, M. and Whitaker, S. Fundamentals of Transport Equation Formulation for Two-Phase Flow in Homogeneous and Heterogeneous Porous Media. In *Vadose Zone Hydrology: Cutting Across Disciplines*, chapter 1, pp. 3–57. Oxford University Press, New York, 1999.
- [92] Hashemi, A. and Shadizadeh, S. R. The Impact of Reservoir Properties on Pseudo Functions: Upscaling of Relative Permeability. *Petroleum Science and Technology*, vol. 32, no. 7, pp. 772–782, 2014.
- [93] Quintard, M. and Whitaker, S. Two-Phase Flow in Heterogeneous Porous Media I: The

- Influence of Large Spatial and Temporal Gradients. *Transport in Porous Media*, vol. 5, pp. 341–379, 1990.
- [94] Hilfer, R. Macroscopic Equations of Motion for Two-Phase Flow in Porous Media. *Physical Review E*, vol. 58, no. 2, pp. 2090–2096, 1998.
- [95] Panfilov, M. and Panfilova, I. Phenomenological Meniscus Model for Two-Phase Flows in Porous Media. *Transport in porous media*, vol. 58, no. 1-2, pp. 87–119, 2005.
- [96] Cueto-Felgueroso, L. and Juanes, R. A Phase Field Model of Unsaturated Flow. *Water Resources Research*, vol. 45, no. 10, pp. 1–23, 2009.
- [97] Buchlin, J. and Stubos, A. Phase Change Phenomena at Liquid Saturated Self Heated Particulate Beds. In *Modelling and Applications of Transport Phenomena in Porous Media*, 221–276. Springer, 1991.
- [98] Fourar, M., Lenormand, R. and Larachi, F. Extending the F-Function Concept to Two-Phase Flow in Trickle Beds. *Chemical Engineering Science*, vol. 56, pp. 5987–5994, 2001.
- [99] Reed, A. The Effect of Channeling on the Dryout of Heated Particulate Beds Immersed in a Liquid Pool. Ph.D. thesis, Massachusetts Institute of Technology, 1982.
- [100] Lipinski, R. J. A Coolability Model for Post Accident Nuclear Reactor Debris. *Nuclear Technology*, vol. 65, pp. 53, 1984.
- [101] Hu, K. and Theofanous, T. On the measurement and mechanism of dryout in volumetrically heated coarse particle beds. *International Journal of Multiphase Flow*, vol. 17, pp. 519–532, 1991.
- [102] Lasseux, D., Ahmadi, A. and Arani, A. Two-Phase Inertial Flow in Homogeneous Porous Media : A Theoretical Derivation of a Macroscopic Model. *Transport in Porous Media*, vol. 75, pp. 371–400, 2008.

- [103] Tutu, N., Ginsberg, T., Klein, J., Klages, J. and Schwarz, C. Debris Bed Quenching Under Bottom Flood Conditions (In-Vessel Degraded Core Cooling Phenomenology) [PWR]. Technical report, Brookhaven National Lab., 1984.
- [104] Clavier, R., Chikhi, N., Fichot, F. and Quintard, M. Two-Phase Flow in Porous Media at High Reynolds Number: Discussion of Macro-Scale Models Based on New Experimental Data. In *ISHT-9, Beijing*, A0207. 2016.
- [105] Lipinski, R. J. A One-Dimensional Particle Bed Dryout Model. *Transactions of the American Nuclear Society*, vol. 38, pp. 386–387, 1981.
- [106] Reed, A.-W., Bergeron, E.-D., Boldt, K.-R. and Schmidt, T.-R. Coolability of UO₂ Debris Beds in Pressurized Water Pools : DCC-1 & DCC-2 Experiment Results. *Nuclear Engineering and Design*, vol. 97, pp. 81–88, 1986.
- [107] Tung, V. and Dhir, V. A Hydrodynamic Model for Two-Phase Flow Through Porous Media. *International Journal of Multiphase Flow*, vol. 14, pp. 47–65, 1988.
- [108] Tung, V. and Dhir, V. On Fluidization of a Particulate Bed During Quenching by Flooding From the Bottom. *Proceedings of the 6th Information Exchange Meeting on Debris Bed coolability*, pp. 14–1–14–13, 1986.
- [109] Taherzadeh, M. and Saidi, M. Modeling of Two-Phase Flow in Porous Media With Heat Generation. *International Journal of Multiphase Flow*, vol. 69, pp. 115–127, 2015.
- [110] Mahr, B. and Mewes, D. CFD Modelling and Calculation of Dynamic Two-Phase Flow in Columns Equipped With Structured Packing. *Chemical Engineering Research and Design*, vol. 85, no. 8, pp. 1112–1122, 2007.
- [111] Mahr, B. and Mewes, D. Two-Phase Flow in Structured Packings: Modeling and Calculation on a Macroscopic Scale. *AIChE Journal*, vol. 54, no. 3, pp. 614–626, 2008.

- [112] Soulaine, C., Davit, Y. and Quintard, M. A Two-Pressure Model for Slightly Compressible Single Phase Flow in Bi-Structured Porous Media. *Chemical Engineering Science*, vol. 96, pp. 55–70, 2013.
- [113] Soulaine, C., Horgue, P., Franc, J. and Quintard, M. Gas–Liquid Flow Modeling in Columns Equipped With Structured Packing. *AIChE Journal*, vol. 60, no. 10, pp. 3665–3674, 2014.
- [114] Fourati, M., Roig, V. and Raynal, L. Liquid Dispersion in Packed Columns: Experiments and Numerical Modeling. *Chemical Engineering Science*, vol. 100, pp. 266–278, 2013.
- [115] Soulaine, C. Modélisation des Écoulements dans les Garnissages Structurés : de l'Échelle du Pore à l'Échelle de la Colonne. Ph.D. thesis, University of Toulouse, 2012.
- [116] Augier, F., Koudil, A., Royon-Lebeaud, A., Muszynski, L. and Yanouri, Q. Numerical Approach to Predict Wetting and Catalyst Efficiencies Inside Trickle Bed Reactors. *Chemical Engineering Science*, vol. 65, no. 1, pp. 255 – 260, 2010.
- [117] Charpentier, J.-C. and Favier, M. Some Liquid Holdup Experimental Data in Trickle-Bed Reactors for Foaming and Nonfoaming Hydrocarbons. *AIChE Journal*, vol. 21, no. 6, pp. 1213–1218, 1975.
- [118] Ng, K. and Chu, C. Trickle-Bed Reactors. *Chemical Engineering Progress*, vol. 83, no. 11, 1987.
- [119] Kondo, M. and Nakajima, K.-I. Experimental Investigation of Air-Water Two Phase Upflow Across Horizontal Tube Bundles: Part 1, Flow Pattern and Void Fraction. *Bulletin of the Japan Society of Mechanical Engineers*, vol. 23, no. 177, pp. 385–393, 1980.
- [120] Melli, T. R., De Santos, J. M., Kolb, W. B. and Scriven, L. Cocurrent Downflow in Networks of Passages. Microscale Roots of Macroscale Flow Regimes. *Industrial & Engineering Chemistry Research*, vol. 29, no. 12, pp. 2367–2379, 1990.

- [121] Horgue, P., Augier, F., Duru, P., Prat, M. and Quintard, M. Experimental and Numerical Study of Two-Phase Flows in Arrays of Cylinders. *Chemical Engineering Science*, vol. 102, pp. 335–345, 2013.
- [122] Raynal, L., Augier, F., Bazer-Bachi, F., Haroun, Y. and da Fonte, C. P. CFD Applied to Process Development in the Oil and Gas Industry—A Review. *Oil & Gas Science and Technology*, vol. 71, no. 3, pp. 42, 2015.
- [123] Sahimi, M. *Applications of Percolation Theory*. CRC Press, 1994.
- [124] Melli, T. R. and Scriven, L. Theory of Two-Phase Cocurrent Downflow in Networks of Passages. *Industrial & Engineering Chemistry Research*, vol. 30, no. 5, pp. 951–969, 1991.
- [125] Joekar-Niasar, V. and Hassanizadeh, S. Analysis of Fundamentals of Two-Phase Flow in Porous Media Using Dynamic Pore-Network Models: A Review. *Critical Reviews in Environmental Science and Technology*, vol. 42, no. 18, pp. 1895–1976, 2012.
- [126] Hannaoui, R., Horgue, P., Larachi, F., Haroun, Y., Augier, F., Quintard, M. and Prat, M. Pore-Network Modeling of Trickle Bed Reactors: Pressure Drop Analysis. *Chemical Engineering Journal*, vol. 262, pp. 334 – 343, 2015.
- [127] Guibert, R., Horgue, P., Debenest, G. and Quintard, M. A Comparison of Various Methods for the Numerical Evaluation of Porous Media Permeability Tensors From Pore-Scale Geometry. *Mathematical Geosciences*, vol. 48, no. 3, pp. 329–347, 2016.



Yohan Davit is Chargé de Recherche CNRS at the Institut de Mécanique des Fluides in Toulouse, France. Prior to joining CNRS, he was a postdoctoral researcher at the Mathematical Institute at the University of Oxford. He received his PhD degree, for which he was awarded the prize Léopold Escande, in 2011 from the University of Toulouse. He studied at the Institut National Polytechnique de Grenoble and the Université Joseph Fourier, where he obtained his MS degree. His research interests include the ecology of biofilms, transport phenomena in biological and porous media, and multiscale approaches for heterogeneous systems.



Michel Quintard is Directeur de Recherche CNRS at the Institut de Mécanique des Fluides in Toulouse, France. Engineer from Top School "Ecole Nationale Supérieure des Arts et Métiers", he received his PhD in fluid mechanics from the University of Bordeaux (1979). His research interests focus on transport phenomena in porous media with fundamental objectives such as the development of macro-scale models through the use of averaging techniques, applied to different scales and different displacement mechanisms (multiphase, multicomponent, phase change, chemical reaction, biodegradation, dissolution, superfluid, . . .), with applications in petroleum engineering, environmental hydrogeology, chemical engineering, nuclear safety, aerospace industry, etc. M. Quintard has co-authored about 190 papers in archival journals. He was awarded a Bronze Medal from CNRS in 1984, the Prize Coron-Thévenet from "Académie des Sciences de Paris" in 1994, and became Chevalier of the "Légion d'Honneur" in 2009 for his action as President of the Scientific Council of IRSN (French Nuclear Safety and Radioprotection Institute).

List of Figures

1	Schematic representation of a porous medium.	49
2	Various flow regimes characterized by the apparent permeability, k^* , as a function of the Reynolds number.	50
3	Porous medium with rough surfaces (from [32]).	51
4	Porous medium with small scale rough surfaces: rough (left) and effective surface simulation (right), adapted from [32].	52
5	Schematic representation of an annular creeping two-phase flow.	53
6	Plot of the different ratios K_{ij}/K for $\frac{\mu_\gamma}{\mu_\beta} = 0.001$	54
7	Experimental and modeling results for the normalized pressure drop versus the gas velocity at $V_\beta = 0$ (from Clavier et al. in [104]).	55
8	Experimental and modeling results for the gas saturation versus the gas velocity at $V_\beta = 0$ ([104]).	56
9	Photograph of structured packings (Wikimedia Commons, author: Luigi Chiesa).	57
10	Saturation $S_{\beta_1} + S_{\beta_2}$ showing the spreading at three different times of a top of column impinging jet (from [115]).	58
11	Saturation $S_{\beta_1} + S_{\beta_2}$ showing the spreading at a given column cross-section of an impinging jet at the top of the column (from [113]): a) experimental results from [114], b-h) numerical results with increasing mass exchange from [113].	59
12	Illustration of 3D simulations for ethanol/alumina systems (mesh and liquid volume fraction snapshots). The fluid flows from the north pole of the top sphere. Taken from [116], Fig. 2.	60
13	Experimental data (left) and numerical solution (right) for two-phase flow in a bundle of cylinders, from [121].	61
14	Schematic representation of a mesoscale hybrid model.	62
15	Results from [126] for saturation (a) and pressure (b) fields.	63

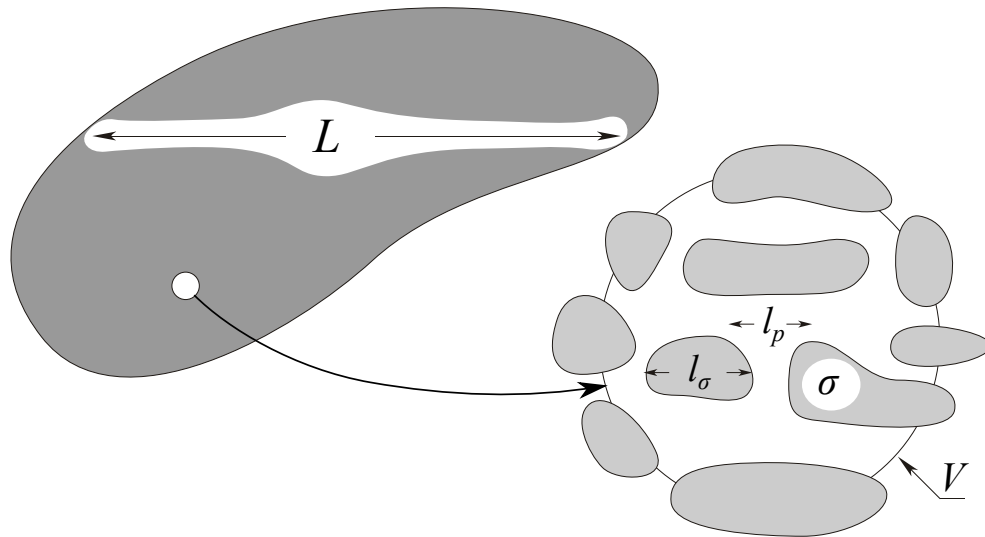


Figure 1: Schematic representation of a porous medium.

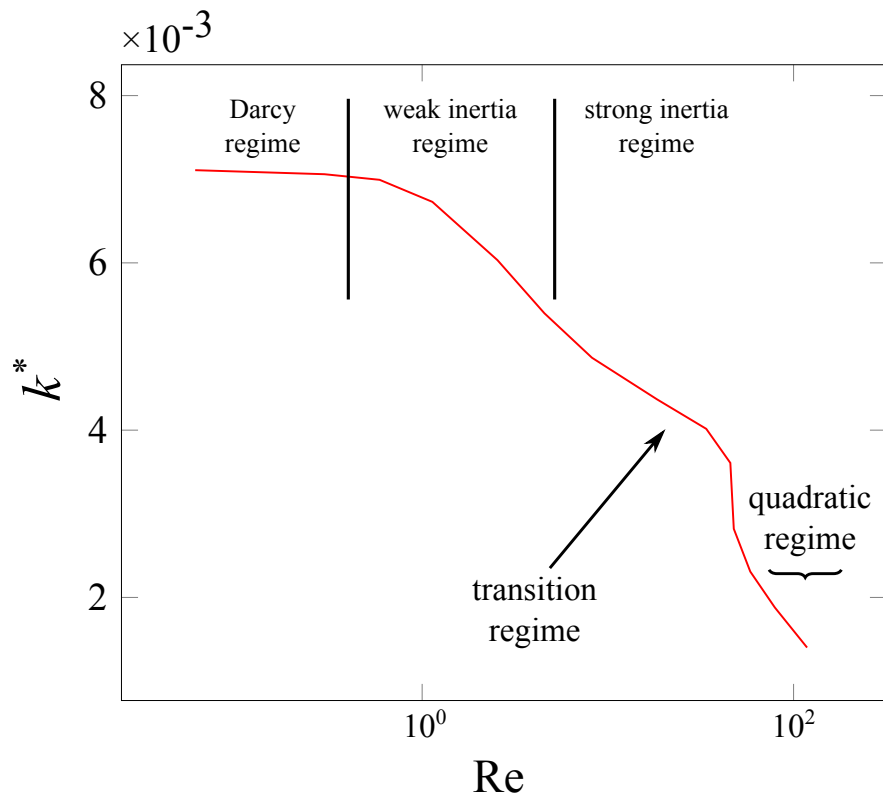


Figure 2: Various flow regimes characterized by the apparent permeability, k^* , as a function of the Reynolds number.

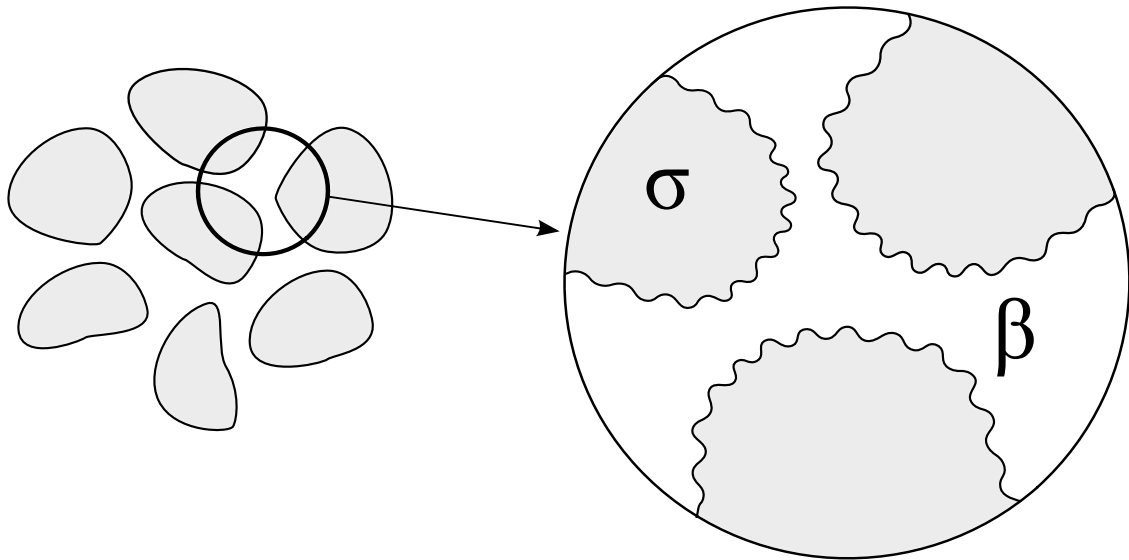


Figure 3: Porous medium with rough surfaces (from [32]).

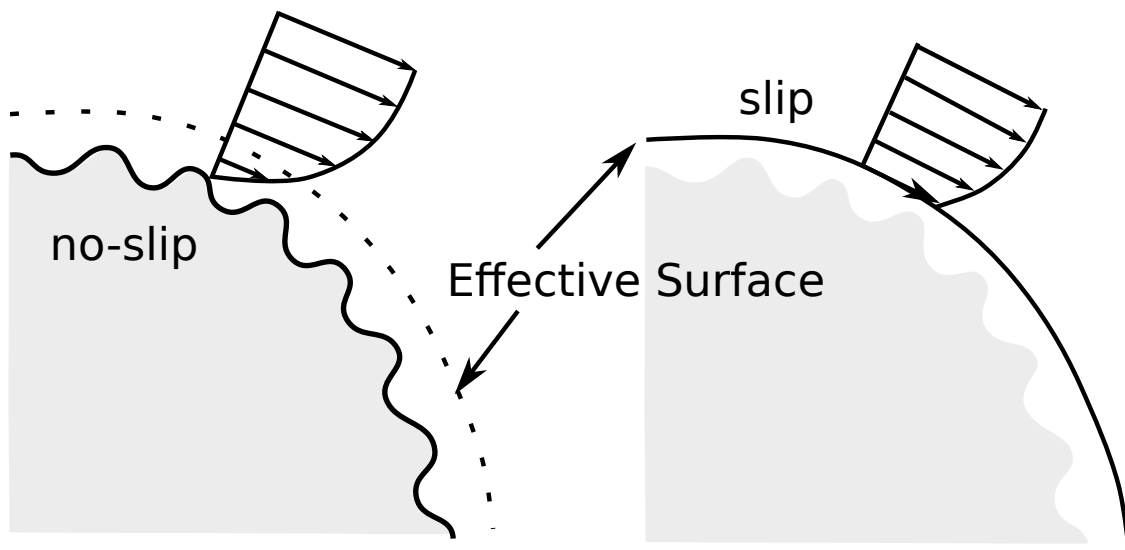


Figure 4: Porous medium with small scale rough surfaces: rough (left) and effective surface simulation (right), adapted from [32].

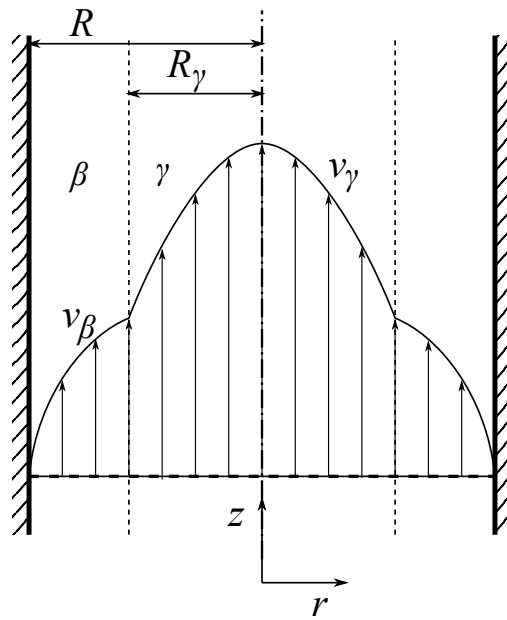


Figure 5: Schematic representation of an annular creeping two-phase flow.

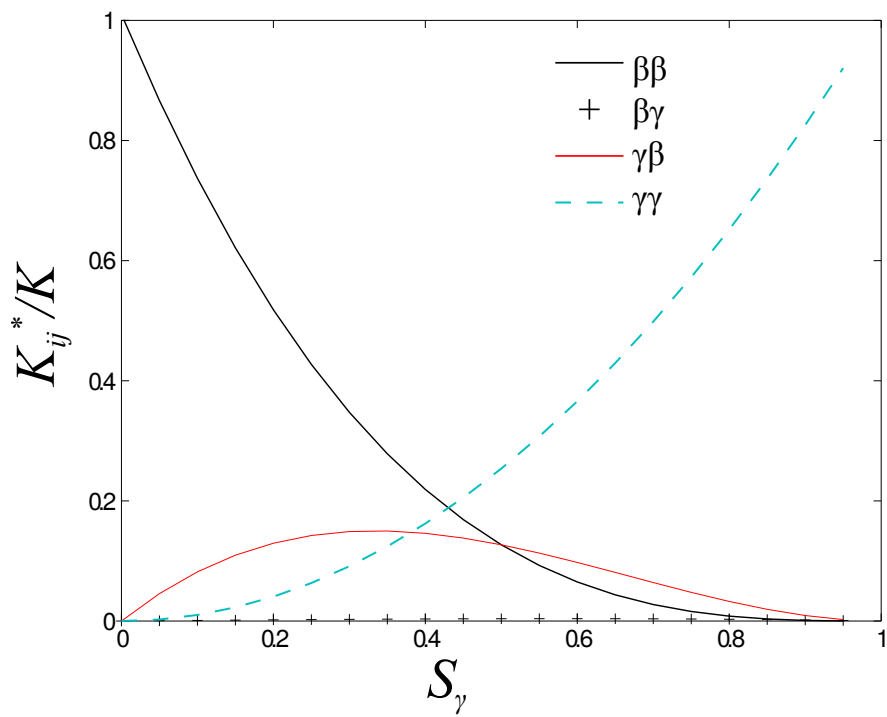


Figure 6: Plot of the different ratios K_{ij}/K for $\frac{\mu_{\gamma}}{\mu_{\beta}} = 0.001$.

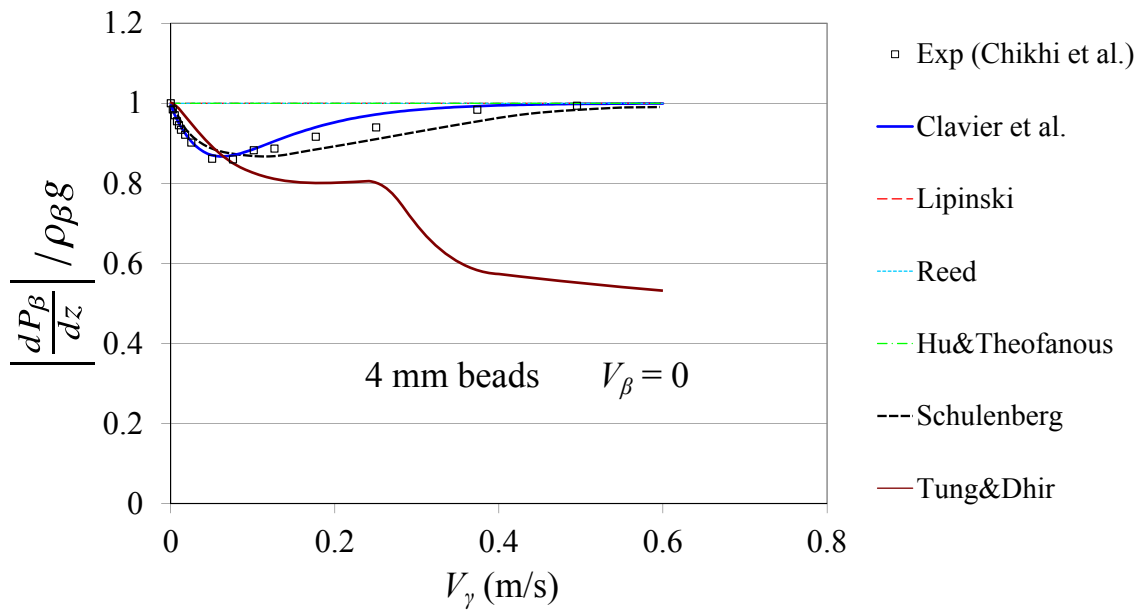


Figure 7: Experimental and modeling results for the normalized pressure drop versus the gas velocity at $V_\beta = 0$ (from Clavier et al. in [104]).

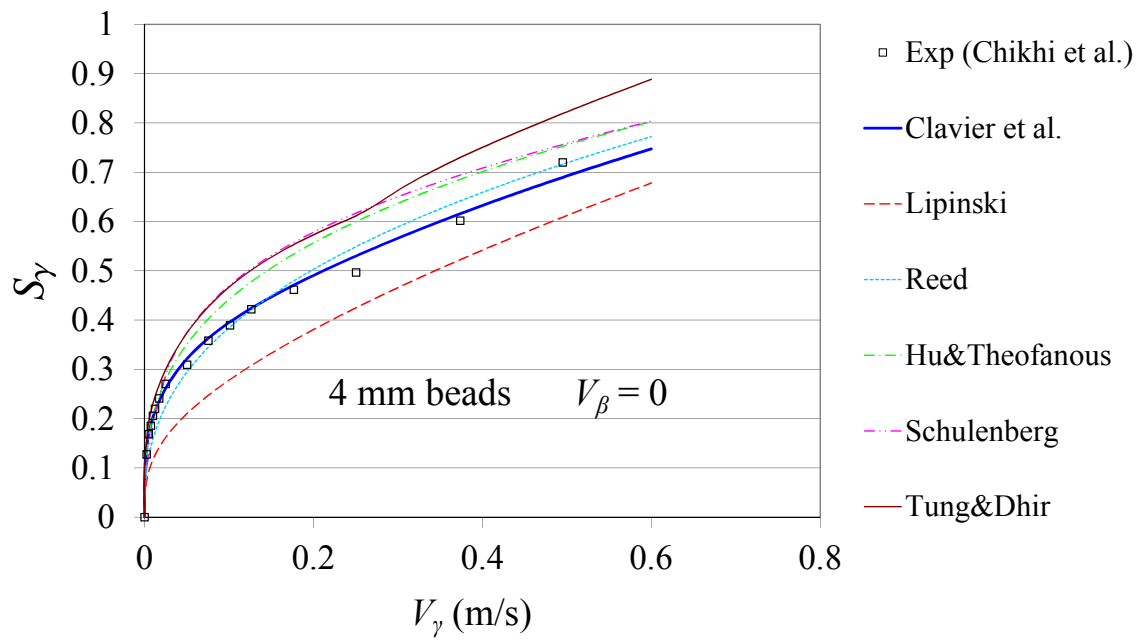


Figure 8: Experimental and modeling results for the gas saturation versus the gas velocity at $V_\beta = 0$ ([104]).



Figure 9: Photograph of structured packings (Wikimedia Commons, author: Luigi Chiesa).

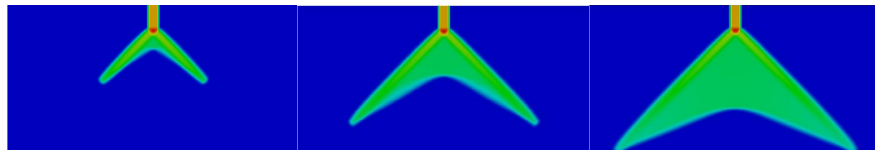


Figure 10: Saturation $S_{\beta_1} + S_{\beta_2}$ showing the spreading at three different times of a top of column impinging jet (from [115]).

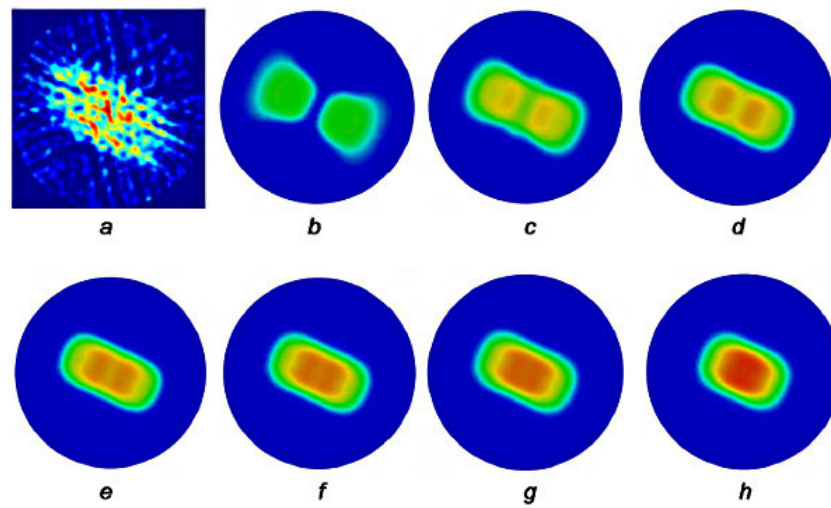


Figure 11: Saturation $S_{\beta_1} + S_{\beta_2}$ showing the spreading at a given column cross-section of an impinging jet at the top of the column (from [113]): a) experimental results from [114], b-h) numerical results with increasing mass exchange from [113].

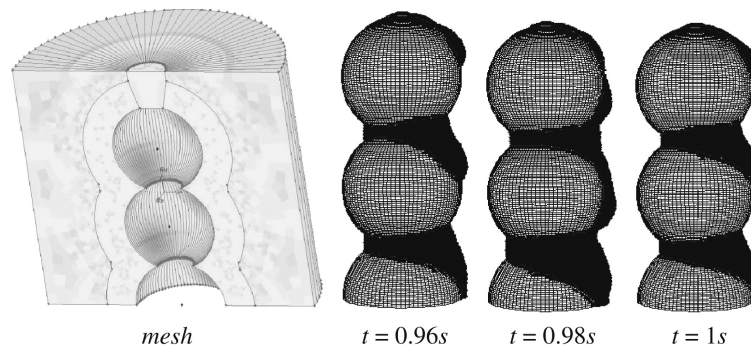


Figure 12: Illustration of 3D simulations for ethanol/alumina systems (mesh and liquid volume fraction snapshots). The fluid flows from the north pole of the top sphere. Taken from [116], Fig. 2.

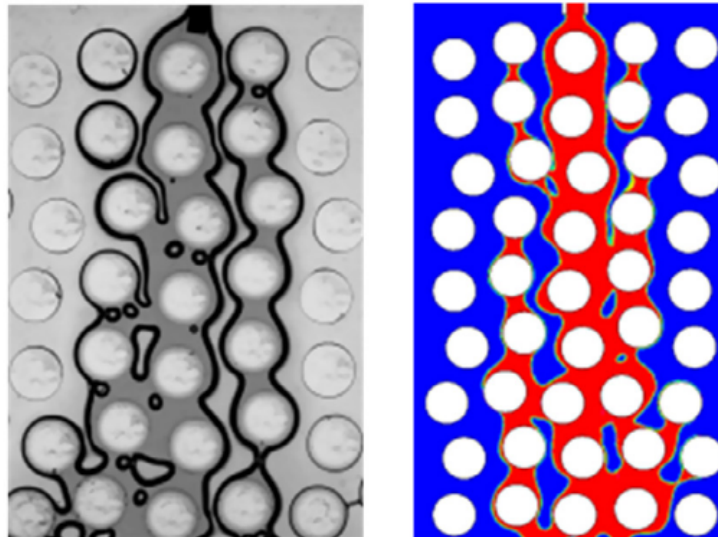


Figure 13: Experimental data (left) and numerical solution (right) for two-phase flow in a bundle of cylinders, from [121].

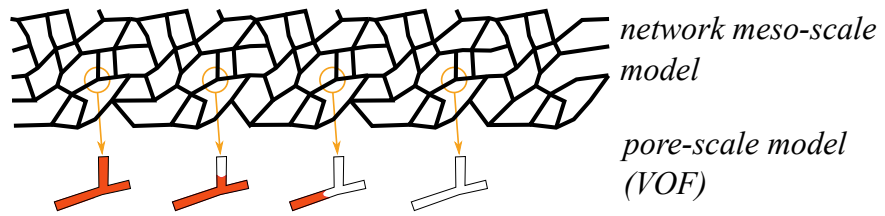


Figure 14: Schematic representation of a mesoscale hybrid model.

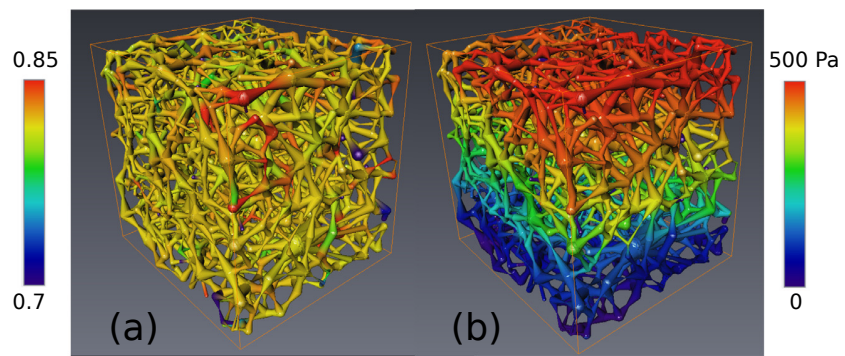


Figure 15: Results from [126] for saturation (a) and pressure (b) fields.